Journal of Medicinal Chemistry

Article

Cite This: J. Med. Chem. 2018, 61, 1576−1594

pubs.acs.org/jmc

Design and Synthesis of Novel Reactive Oxygen Species Inducers for the Treatment of Pancreatic Ductal Adenocarcinoma

Yuting Kuang,[†,§] Mario Sechi,[*,¶] Salvatore Nurra,[¶] Mats Ljungman,[⊥] and Nouri Neamati[*,†]

[†]Department of Medicinal Chemistry, College of Pharmacy, University of Michigan, 1600 Huron Parkway, Ann Arbor, Michigan 48109, United States

[§]Department of Pharmacology and Pharmaceutical Sciences, School of Pharmacy, University of Southern California, 1985 Zonal Avenue, Los Angeles, California 90033, United States

[¶]Department of Chemistry and Pharmacy, University of Sassari, Via Vienna 2, 07100 Sassari, Italy

[⊥]Department of Radiation Oncology, University of Michigan, 1600 Huron Parkway, Ann Arbor, Michigan 48109, United States

Supporting Information

ABSTRACT: Altering redox homeostasis provides distinctive therapeutic opportunities for the treatment of pancreatic cancer. Quinazolinediones (QDs) are novel redox modulators that we previously showed to induce potent growth inhibition in pancreatic ductal adenocarcinoma (PDAC) cell lines. Our lead optimization campaign yielded **QD325** as the most potent redox modulator candidate inducing substantial reactive oxygen species (ROS) in PDAC cells. Nascent RNA sequencing following treatments with the QD compounds revealed induction of stress responses in nucleus, endoplasmic reticulum, and mitochondria of pancreatic cancer cells. Furthermore, the QD compounds induced Nrf2-mediated oxidative stress and unfolded protein responses as demonstrated by dose-dependent increases in RNA synthesis of representative genes such as *NQO1, HMOX1, DDIT3*, and *HSPA5*. At higher concentrations, the QDs blocked mitochondrial function by inhibiting mtDNA transcription and downregulating the mtDNA-encoded OXPHOS enzymes. Importantly, treatments with **QD325** were well tolerated *in vivo* and significantly delayed tumor growth in mice. Our study supports the development of **QD325** as a new therapeutic in the treatment of PDAC.

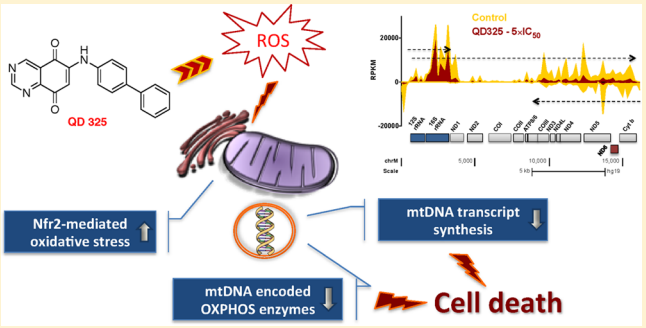

INTRODUCTION

Pancreatic cancer is the fourth leading cause of cancer-related death in both genders in the United States, estimated to claim over 40 000 lives in 2017.[1] Given its asymptomatic and metastatic nature, over 50% of pancreatic cancer cases are diagnosed at late stages, when the tumor has metastasized and is often unresectable.[2] Therefore, treatment of pancreatic cancer is largely dependent on systemic chemotherapy. Ever since its approval by the FDA in 1996, gemcitabine-based regimes have been the standard of care for pancreatic cancer.[3] However, limited by late-stage diagnosis and inherent/acquired resistance to available chemotherapy, the overall five-year survival rate of pancreatic cancer is only 6.7%, one of the lowest among all types of cancers. Recently, two combination regimens with modest clinical activity have been added as an option for pancreatic cancer patients. The combination of nab-paclitaxel (albumin-bound paclitaxel) with gemcitabine has increased median overall survival from 6.7 to 8.5 months.[4] The combination cocktail including oxaliplatin, irinotecan, fluorouracil, and leucovorin (FOLFIRINOX) was approved for the treatment of metastatic pancreatic cancer by improving median overall survival from 6.8 months in the gemcitabine group to 11.1 months in the FOLFIRINOX group,[5] but increased toxicity is the major concern for these new treatment options.[6−8] Therefore, novel therapeutics are urgently needed to enhance the survival and quality of life of patients with this devastating disease.[9−11]

Modulation of redox homeostasis in cancer cells provides a new opportunity for tumor intervention.[12−18] Reactive oxygen species (ROS), natural byproducts from mitochondrial respiration and other cellular processes, play important roles as second messengers in cell signaling.[19] However, when present at high concentrations, ROS can be detrimental to cells by inducing oxidative damage to DNA, lipids, and proteins.[20] Cells eliminate excess intracellular ROS via expression of antioxidant genes regulated by the ROS-detoxifying machinery. In tumor cells, antioxidant enzymes are often induced as a result of elevated levels of intrinsic ROS.[21] Expression of mutant oncogenic $Kras^{G12D}$, commonly present in pancreatic ductal adenocarcinoma (PDAC), keeps the master transcription factor NRF2 elevated at basal state to mount an antioxidant response.[22−25] A shift in the redox homeostasis is expected to make tumor cells more susceptible to induced oxidative stress, overwhelming their adaptive antioxidant capacity and promoting ROS-mediated cell death.[26−28]

Received: October 24, 2017
Published: January 12, 2018

DOI: 10.1021/acs.jmedchem.7b01463
J. Med. Chem. 2018, 61, 1576−1594

Among various classes of small-molecule drugs tested in our laboratory to induce ROS, the quinone containing compounds showed great promise due to their significant increase in oxygen consumption rate in treated cells. Many quinones inhibit multiple biochemical assays due to their redox, metal-chelation, color, and in some cases, reactivity toward nucleophiles through Michael addition. Therefore, they are classified as pan assay inhibitors in high throughput screening campaigns. However, over two-dozen drugs containing a quinone moiety have been approved by the FDA or are under clinical investigations not only in oncology but also for other diseases. For example, doxorubicin and dozen of its analogues, mitoxantrone, and mitomycin C are some of the most commonly used FDA approved chemotherapeutic agents for numerous cancers that contain a quinone group. In addition, there are many other agents that are approved for various indications or are in late stage clinical development that broadly fall under the quinone class of drugs (Chart 1).

Previously, we showed that the quinazolinedione **QD232** (Chart 2) exerts ROS-mediated cytotoxicity in pancreatic cancer models.[29,30] In this study, we performed a lead optimization campaign and identified **QD325** as a lead compound for in-depth preclinical and mechanistic studies. Several major modifications on **QD232** were made by varying the substituents at the nitrogen atom on position 6 of the quinazoline-5,8-dione backbone.

Specifically, mono/poly substitution on the phenyl ring with various functionalities and/or bulky aromatic system was mainly explored to modulate lipophilicity and steric effects (Chart 2).

Chart 2. Structure of Lead Compound QD232 and Design of Title Compounds

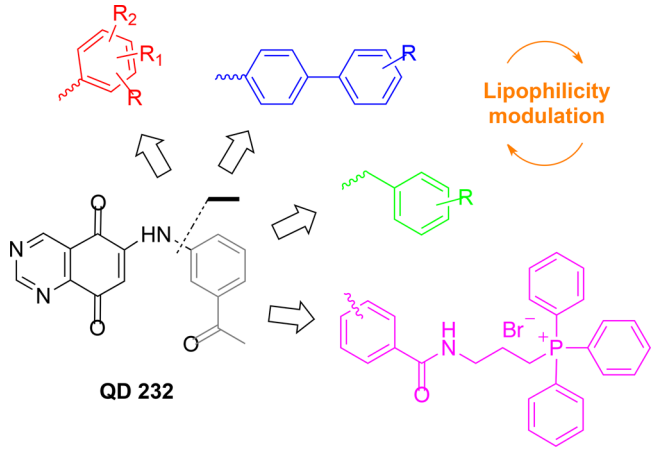

Furthermore, to evaluate a potential synergistic effect in terms of ROS modulation, we sought to conjugate the quinazoline-5,8-dione scaffold to a highly lipophilic triphenylphosphonium cation for mitochondrial targeting.[31,32] Disruption of mitochondrial-mediated cell redox modulation represents a promising avenue for future therapy in cancer. Because our compounds increase ROS production, we tested their ability to interfere with mitochondrial processes.

Chart 1. Select Examples of Drugs Containing Quinone or a Michael Acceptor That Are FDA-Approved or under Clinical Investigations for Various Diseases

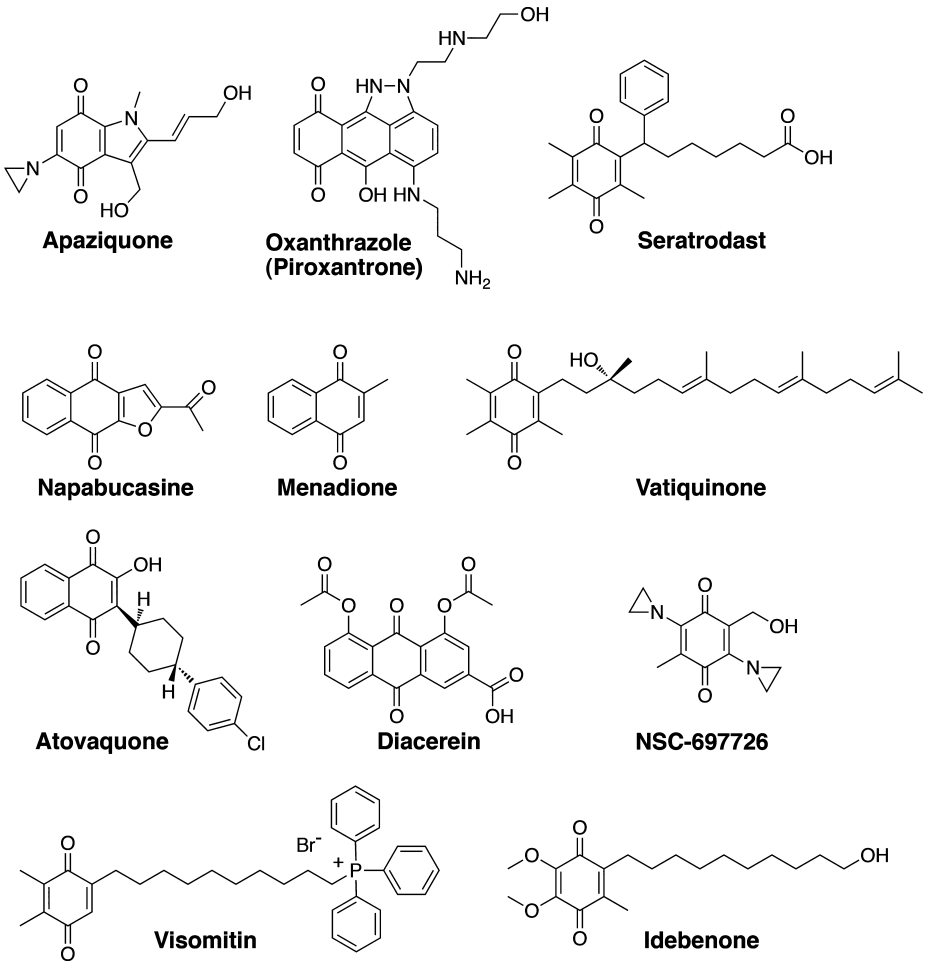

DOI: 10.1021/acs.jmedchem.7b01463
J. Med. Chem. 2018, 61, 1576−1594

Our results show that **QD325** caused selective inhibition of transcription of the mitochondrial genome potentially by abrogating the mitochondrial D-loop, critical for mtDNA transcription. We propose that such targeting could be efficacious and should be further explored as an innovative therapeutic approach to target cancers that heavily depend on mitochondrial function. Importantly, **QD325** was found to be well tolerated and showed tumor-suppressing activities in a pancreatic cancer xenograft model.

RESULTS

Chemistry. The synthesis of compounds **QD324−338, 353−357** (Table 1) was carried out using Bracher's methodology, according to our previously reported procedure with some modifications. Scheme 1 illustrates the synthesis of the key synthone **QD323** from the readily available dimethoxybenzaldehyde (**1**). Nitration of compound **1** with concentrated nitric acid in the presence of acetic anhydride under simple magnetic stirring afforded the 3,6-dimethoxy-2-nitrobenzaldehyde (**2**) in good yield. This regioisomer was converted to the diformamido-derivative **3** under gaseous HCl. Compound **3** was then cyclized to dimethoxyquinazoline **4** by treatment with zinc powder and acetic acid.

Scheme 1. Synthetic Route for the Preparation of the Key Intermediate QD323[a]

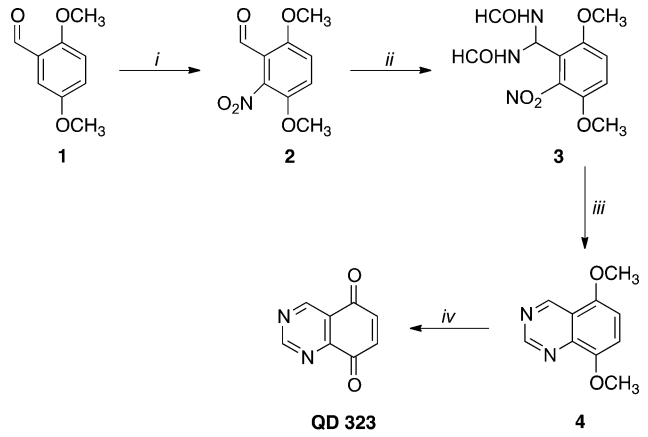

[a]Reagents and conditions: (*i*) conc. HNO_3, $(CH_3CO)_2O$, 0 °C, 1.5 h; (*ii*) H_2NCHO, $HCl_{(g)}$ from 40 to 80 °C, 1h; (*iii*) glacial CH_3COOH, Zn, 0 °C for 2 h, rt for 4 h; (*iv*) $(NH_4)_2Ce(NO_3)_6$, CH_3CN/H_2O, 0 °C, 20 min.

Table 1. Structure and Cytotoxicity of QD Compounds in MIA PaCa-2, Panc-1, and BxPC-3 Cells by MTT Assay[a]

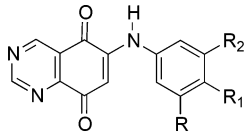

QD 232, 324-338, 340, 353-357, 359

	substitution group			IC $_{50}$ (μM)[b]		
ID	R	R_1	R_2	MIA PaCa-2	Panc-1	BxPC-3
232	$COCH_3$	H	H	2.3 ± 0.2	0.9 ± 0.2	5.2 ± 0.8
325	H	Ph	H	0.9 ± 0.2	0.4 ± 0.1	0.5 ± 0.1
335	H	4-Et-Ph	H	2.0 ± 0.1	1.2 ± 0.1	3.1 ± 0.7
336	H	4-OCH_3−Ph	H	2.1 ± 0.5	2.3 ± 0.3	3.5 ± 0.5
337	H	4-NH_2−Ph	H	2.5 ± 0.2	3.7 ± 0.1	3.5 ± 0.6
334	H	4-F-Ph	H	3.5 ± 1.0	3.2 ± 0.8	4.4 ± 0.9
338	F	4-CH_3−Ph	H	4.6 ± 1.1	4.8 ± 0.1	5.0 ± 0.7
326	OCH_3	OCH_3	OCH_3	1.5 ± 0.1	0.8 ± 0.1	1.6 ± 0.3
353	H	H	OCH_3	1.8 ± 0.3	0.6 ± 0.1	1.8 ± 0.1
354	H	OCH_3	H	1.9 ± 0.2	0.8 ± 0.2	1.7 ± 0.2
355	H	OCH_3	OCH_3	1.8 ± 0.1	0.9 ± 0.3	1.5 ± 0.2
357	OCH_3	H	OCH_3	7.7 ± 2.0	7.2 ± 0.8	16.3 ± 1.5
327	H	OCF_3	H	1.4 ± 0.2	0.9 ± 0.1	0.9 ± 0.1
324	H	O-Ph	H	3.7 ± 0.7	1.8 ± 0.2	3.6 ± 0.4
328	H	SO_2NH_2	H	>10	>10	>10
333	$B(OH)_2$	H	H	>10	9.0 ± 1.0	>10
331	H	$COOCH_3$	H	2.2 ± 0.4	1.1 ± 0.4	5.8 ± 0.3
329	H	CH_2OH	H	3.5 ± 1.3	1.0 ± 0.2	5.7 ± 0.3
332	H	$COOCH_2CH_3$	H	5.5 ± 1.5	1.6 ± 0.3	5.9 ± 0.1
330	H	$CONH_2$	H	8.0 ± 0.9	6.3 ± 0.3	>10
323[c]	N/A	N/A	N/A	9.4 ± 0.9	18.0 ± 2.5	19.4 ± 1.6
356[d]	N/A	N/A	N/A	1.7 ± 0.2	1.0 ± 0.1	1.4 ± 0.2
339[e]	N/A	N/A	N/A	>30	>30	>30
358[f]	N/A	N/A	N/A	>30	>30	>30
331	H	$COOCH_3$	H	2.2 ± 0.4	1.1 ± 0.4	5.8 ± 0.3
340	H $CONH(CH_2)_3(TPP)^+Br^-$[f]		H	15.3 ± 2.5	11.7 ± 1.5	21.5 ± 2.3
232	$COCH_3$	H	H	2.3 ± 0.2	0.9 ± 0.2	5.2 ± 0.8
359	$CONH(CH_2)_3(TPP)^+Br^-$[g] H		H	16.3 ± 3.5	14.3 ± 1.5	21.3 ± 2.5

[a]QD compounds are grouped by structure. [b]Data is presented as mean ± SD from three independent experiments. [c]Structure of intermediate **QD323** is shown in Scheme 1. [d]Structure of **QD356** is shown in Scheme 3. [e]Structure of intermediate **QD339** is shown in Scheme 4. [f]Structure of intermediate **QD358** is shown in Scheme 5. [g]TPP stands for triphenylphosphonium.

DOI: 10.1021/acs.jmedchem.7b01463
J. Med. Chem. 2018, 61, 1576−1594

Final oxidation by cerium ammonium nitrate resulted in the production of quinazoline-5,8-dione **QD323**. Regioselective addition of appropriate aminobenzenes to 6 position of **QD323** in the presence of Ce(III) ions gave **QD324−338**, **353−357** (Schemes 2 and 3).

Scheme 2. Preparation of Compounds QD324−338, 353−355, 357[a]

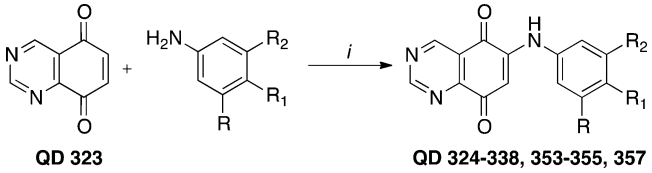

[a]Reagents and conditions: (*i*) $CeCl_3 \cdot 7H_2O$, abs EtOH, rt, 1−6 h.

Scheme 3. Preparation of QD356[a]

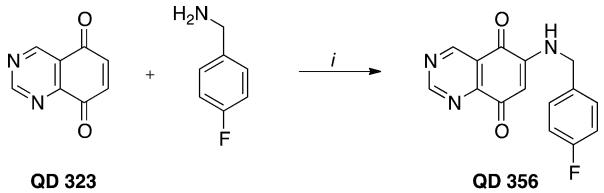

[a]Reagents and conditions: (*i*) $CeCl_3 \cdot 7H_2O$, abs EtOH, rt, 2 h.

Then, we wanted to obtain triphenylphosphonium-based model derivatives of compound **QD331** and **QD232**. Compounds **QD340** and **QD359** were therefore generated by adapting a phosphine conjugation method, as we previously described.[31−33] The synthesis of triphenylphosphonium-based compounds **QD340** and **QD359** is illustrated in Schemes 4 and 5. Initially, 3-bromopropylamine hydrobromide (**5**) was reacted with triphenylphosphine in refluxing acetonitrile for 16 h, and the resulting triphenylphosphonium intermediate (**6**) was isolated after treatment with *n*-hexane/diethyl ether/isopropanol. Next, the 4- and 3-aminobenzamido-propyl-triphenylphosphonium bromides **QD339** and **QD358** were prepared by conjugating **6** with 4- or 3-aminobenzoic acid, respectively, via a standard coupling protocol using DIPEA, HBtU, DMAP, in CH_2Cl_2. Finally, **QD340** and **QD359** were obtained by nucleophilic addition of appropriate triphenylphosphonium salts (**QD339** or **QD358**) to **QD323** in the presence of Ce(III), according to the above-mentioned procedure.

QD Compounds Inhibit Proliferation of Pancreatic Cancer Cells. We designed and synthesized 25 new analogues of our previous lead compound, **QD232**, to better elucidate their mechanisms of action. Nine of these novel analogues showed improved cytotoxicity compared to **QD232** in at least two PDAC cell lines in MTT assay (Table 1). **QD325** was found to be the most potent analogue with IC_{50} values <1 μM in the three PDAC cell lines (MIA PaCa-2, Panc-1, and BxPC-3).

QD325 (as well as **QD232**) showed similar dose-dependent cytotoxicity in MIA PaCa-2 and a gemcitabine-resistant derivative cell line MIA PaCa-2-GR[34] (Table 2). In HPV16-E6E7 immortalized pancreatic cell line HPDE,[35] gemcitabine produced similar IC_{50} values as MIA PaCa-2 cells, while the most potent **QD325** compound showed a 3-fold higher sensitivity for MIA PaCa-2 (Table 2).

Cytotoxicity of QD Compounds Correlates with Increased ROS Production. Treatment with the QD compounds elicited significant ROS accumulation in MIA PaCa-2 cells as shown in the H2DCFDA reactivity assay (Figures 1 and S2). To validate ROS induction as the mechanism for cytotoxicity, the effect of QD compounds was evaluated in the presence and absence of the antioxidant N-acetyl-cysteine (NAC). For the lead compound **QD232** and the two active analogues **QD325** and **QD326**, we observed a time- and dose-dependent accumulation of ROS (Figure 1A). While H_2O_2 treatment lead to an immediate conversion of H2DCFDA to fluorescent DCF, treatment with the QD compounds resulted in a gradual induction of the fluorescent signal, which reached peak levels after 4−6 h, implying a progressive ROS accumulation.

When cells were pretreated with 5 mM NAC, ROS induction by H_2O_2 and the QD compounds was blocked (Figure 1B). In the MTT cell proliferation assay, NAC attenuated the proliferation inhibitory effect of H_2O_2, **QD232**, **QD325**, and **QD326** (Figure 1C). Importantly, we did not observe any colloidal behavior or aggregation for QD compounds in our assays. These results demonstrate that ROS accumulation is a major mechanism for cytotoxicity of the QD compounds. However, NAC treatment did not completely block the effect of the QD compounds and H_2O_2, suggesting these compounds may induce additional cellular effects responsible for the inhibition of cell proliferation. Testing many

Scheme 4. Preparation of QD339, 340[a]

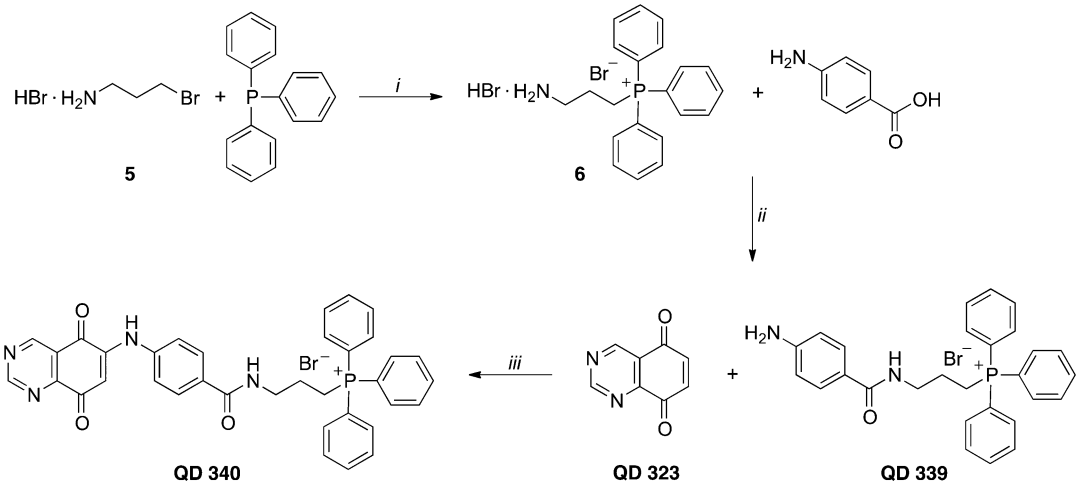

[a]Reagents and conditions: (*i*) MeCN, reflux, 16 h; (*ii*) 4-aminobenzoic acid, DIPEA, HBtU, DMAP, CH_2Cl_2, rt, 5 h; (*iii*) $CeCl_3 \cdot 7H_2O$, abs EtOH, rt, 2 h.

DOI: 10.1021/acs.jmedchem.7b01463
J. Med. Chem. 2018, 61, 1576−1594

Scheme 5. Preparation of QD358, 359[a]

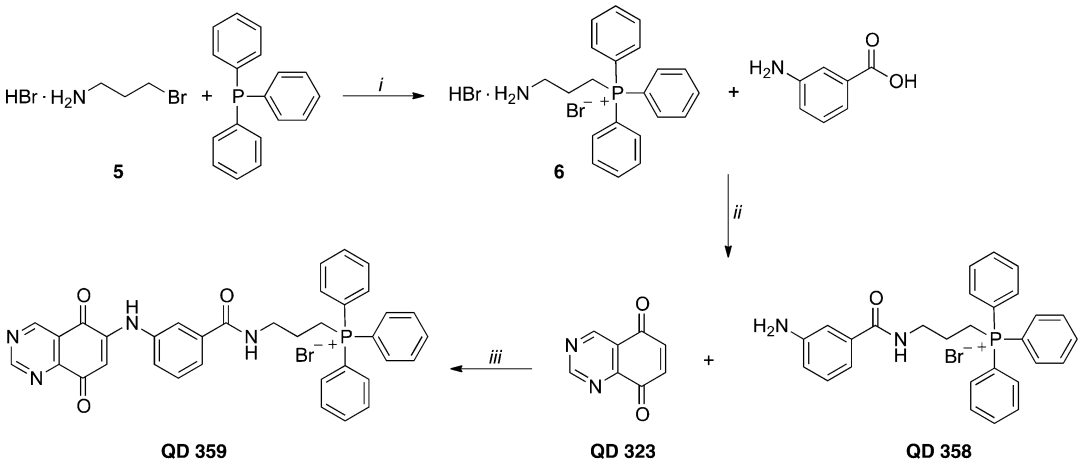

[a]Reagents and conditions: (*i*) MeCN, reflux, 16 h; (*ii*) 3-aminobenzoic acid, DIPEA, HBtU, DMAP, CH_2Cl_2, rt, 5 h; (*iii*) $CeCl_3{\cdot}7H_2O$, abs EtOH, rt, 1.5 h.

Table 2. Cytotoxicity of QD Compounds in Gemcitabine Resistant MIA PaCa-2 cells and Normal Pancreatic Cells by MTT Assay

	IC $_{50}$ (μM)[a]		
ID	MIA PaCa-2	MIA PaCa-2-GR	HPDE
232	2.3 ± 0.2	3.6 ± 0.6	4.5 ± 0.6
325	0.9 ± 0.2	1.0 ± 0.3	2.7 ± 0.3
326	1.5 ± 0.1	2.0 ± 0.1	3.2 ± 0.4
340	15.3 ± 2.5	17.7 ± 1.8	18.3 ± 2.1
359	16.3 ± 3.5	16.2 ± 1.9	24.3 ± 1.2
gemcitabine	0.11 ± 0.07	3.3 ± 0.6	0.14 ± 0.05

[a]Data is presented as mean ± SD from three independent experiments.

analogues in the presence of NAC and GSH at 1 to 5 mM we discovered that these antioxidants could protect toxicity anywhere from 10 to 80% depending on the analogue. In most cases, NAC addition never fully protects the cells even at 1000-fold excess of antioxidant. These studies suggest that the compounds not only produce ROS but also bind to unique targets. It is also possible that the QD-NAC conjugate is partially responsible for the ROS induction and cytotoxicity.

The faster induction of oxidative stress by the optimized compounds is perhaps due to improved membrane permeability (predicted cLogP values for **QD232** and **QD325** are 1.99 and 3.89, respectively). We expected that better in vitro antiproliferative activity of **QD325** should translate to better *in vivo* efficacy. Therefore, we selected **QD325** for extensive mechanistic and *in vivo* studies.

In order to selectively target these compounds to the mitochondria, we synthesized two derivatives containing a triphenylphosphine group. To our surprise, **QD340** and **QD359** did not show better ROS induction and cytotoxicity than **QD325** and were not further explored. A possible explanation of this unexpected behavior could be attributed to their redox properties, because we previously showed that triphenylphosphoniums decreased cellular oxygen consumption rate (OCR). Furthermore, the QD compounds without the triphenylphosphonium group cause a remarkable increase in cellular OCR.[30]

QD Compounds Induce Oxidative Stress and the Unfolded Protein Response. We used the recently established bromouridine labeled RNA sequencing (Bru-seq) technique to better characterize transcriptional effects of the QD compounds. Bru-seq captures nascent RNA and provides information on ongoing transcription genome-wide without interference by pre-existing RNA.[36,37] We observed that the transcription signatures induced by 4-h treatments with **QD232** or **QD325** were similar according to Ingenuity Pathway Analysis (IPA) or Gene Set Enrichment Analysis (GSEA) of the expressed genes (Figures 2 and S3−S6). This implies that the two compounds have similar mechanisms of action. IPA profiling of all genes with >1.5-fold change in expression upon treatment of MIA PaCa-2 cells with **QD232** or **QD325** identified the "NRF2-mediated oxidative stress response" and "unfolded protein response" (UPR) as key pathways activated by these compounds (Figure 2A).

NRF2 is a transcription factor that is rapidly activated in response to oxidative and electrophilic exposure, and it promotes the transcription of genes encoding various detoxifying enzymes.[38] Upon oxidative challenge, KEAP1 inactivation allows nascent NRF2 proteins to translocate to the nucleus[39,40] and activate transcription of antioxidant genes containing AREs (antioxidant response element) or MAREs (MAF recognition element) in *cis*-acting enhancer elements.

NQO1 and *HMOX1* are two target genes of NRF2 that counteract the effects of oxidative stress.[41,42] *NQO1* encodes the flavoprotein NAD(P)H:quinone oxidoreductase 1 that catalyzes a two-electron reduction of quinones to hydroquinones and exhibits chemo-protective effects.[43,44] *HMOX1* encodes heme oxygenase 1 (HO-1), whose antioxidant properties arise from degradation of the pro-oxidant heme and production of antioxidant bilirubin from biliverdin.[45] As revealed by Bru-seq, synthesis of *NQO1* and *HMOX1* RNAs was upregulated in a dose-dependent manner by treatments with either **QD232** or **QD325** (Figure 2B).

The unfolded protein response (UPR) comprises three pathways regulated by the ER trans-membrane proteins inositol-requiring enzyme 1a (IRE1a), activating transcription factor 6 (ATF6), and protein kinase RNA-like endoplasmic reticulum kinase (PERK), respectively.[46−48] Misfolded proteins in the ER lumen trigger the competitive binding of the ER chaperone GRP78, leading to the activation of IRE1a, ATF6 and PERK and downstream responses to UPR.[49] Depending on the severity and duration of the ER stress, the UPR can function as a pro-survival mechanism and restore homeostasis, or trigger apoptosis if the stress burden is beyond the capacity of this adaptive response.[50,51]

DDIT3 and *HSPA5* are genes that are induced as a result of UPR signaling. *HSPA5* encodes GRP78, the key regulatory protein of ER stress. *DDIT3* is a downstream target gene that

DOI: 10.1021/acs.jmedchem.7b01463
J. Med. Chem. 2018, 61, 1576−1594

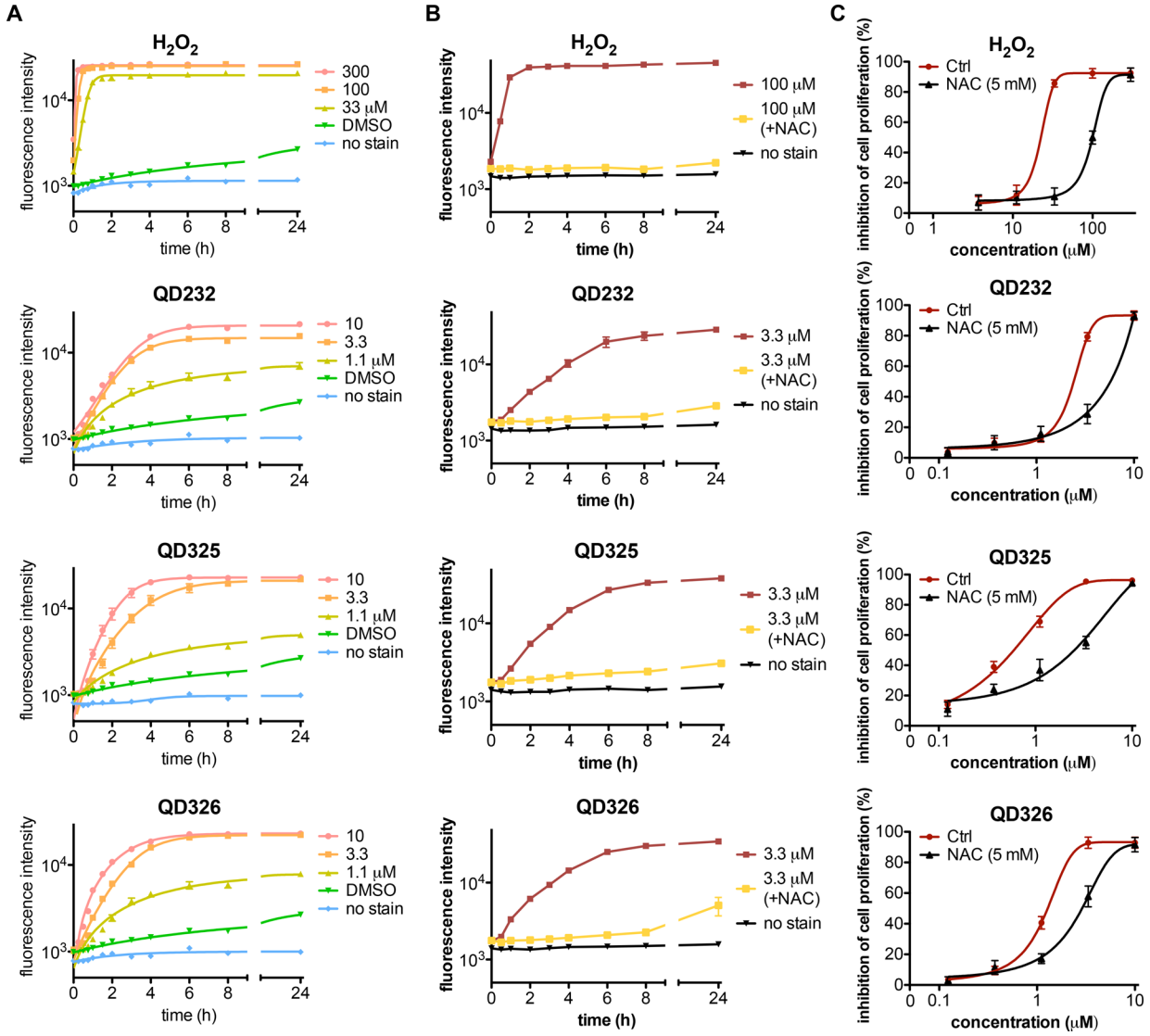

Figure 1. Cytotoxicity of the QD compounds is reduced by NAC in MIA PaCa-2 cells. (A) The parental compound **QD232** induces ROS accumulation in a dose- and time-dependent manner. The new analogues **QD325** and **QD326** induced a stronger and more rapid ROS accumulation in MIA PaCa-2 cells than the parental **QD232** compound. Compounds were tested at 10, 3.3, or 1.1 μM. DMSO was used as a negative control to determine the basal signal of the assay (DMSO). Cells without preloaded H2DCFDA were treated with compounds at 10 μM at the same conditions to determine the endogenous fluorescence of the compounds (no stain). Data points represent mean ± SD from duplicates. Graphs are representatives of three independent experiments. (B) ROS induction by **QD232**, **325**, and **326** was inhibited by NAC pretreatment (5 mM for 30 min). Data points represent mean ± SD from duplicates. Graphs are representatives of three independent experiments. (C) Presence of NAC at 5 mM decreased the cytotoxicity of the **QD232**, **QD325**, and **QD326** compounds. Cytotoxicity was determined by the MTT assay after a 72 h treatment. Data points represent mean ± SD from three independent experiments.

transcriptionally responds to all three arms of the UPR. As a transcription factor, the *DDIT3* gene product CHOP promotes apoptosis under prolong ER stress by inducing transcription of pro-apoptotic genes including PUMA and BIM.[52−54] Transcription of the two stress-responsive genes *DDIT3* and *HSPA5* is significantly increased by **QD232** or **QD325** treatment in a dose-dependent manner (Figure 2C).

Upregulation of mRNA synthesis detected by Bru-seq was found to also result in increased protein levels of the major stress responsive genes. We observed time-dependent increased protein levels of CHOP and GRP78 in MIA PaCa-2, Panc-1, and BxPC-3 cells treated with the QD compounds (Figure 3A−C). For the oxidative stress responsive genes, *HO-1* was upregulated by QD treatments in MIA PaCa-2 and BxPC-3 cells, while no significant change was detected in Panc-1 cells. Of note, the *NQO1* gene is known to be deleted in Panc-1 cells, and as expected, no transcription of the gene was observed in this cell line using Bru-seq In MIA PaCa-2 and BxPC-3, *NQO1* showed high basal expression levels with no further induction following treatment. These results suggest that MIA PaCa-2 and BxPC-3 cells have a high intrinsic oxidative stress burden and that this may make them sensitive to exogenous agents inducing oxidative stress. Indeed, IPA analysis showed significant activation of apoptosis signaling at higher concentration of **QD232** (3 times IC_{50}) or **QD325** (5 times IC_{50}) after 4 h treatment (Figure S3), suggesting that apoptosis is a mode of death following exposure to the QD compounds.

Previously, it was shown that ROS-inducing compounds such as phenethylisothiocyanate and curcumin efficiently downregulate specificity protein (Sp) transcription factors Sp1, Sp3,

DOI: 10.1021/acs.jmedchem.7b01463
J. Med. Chem. 2018, 61, 1576−1594

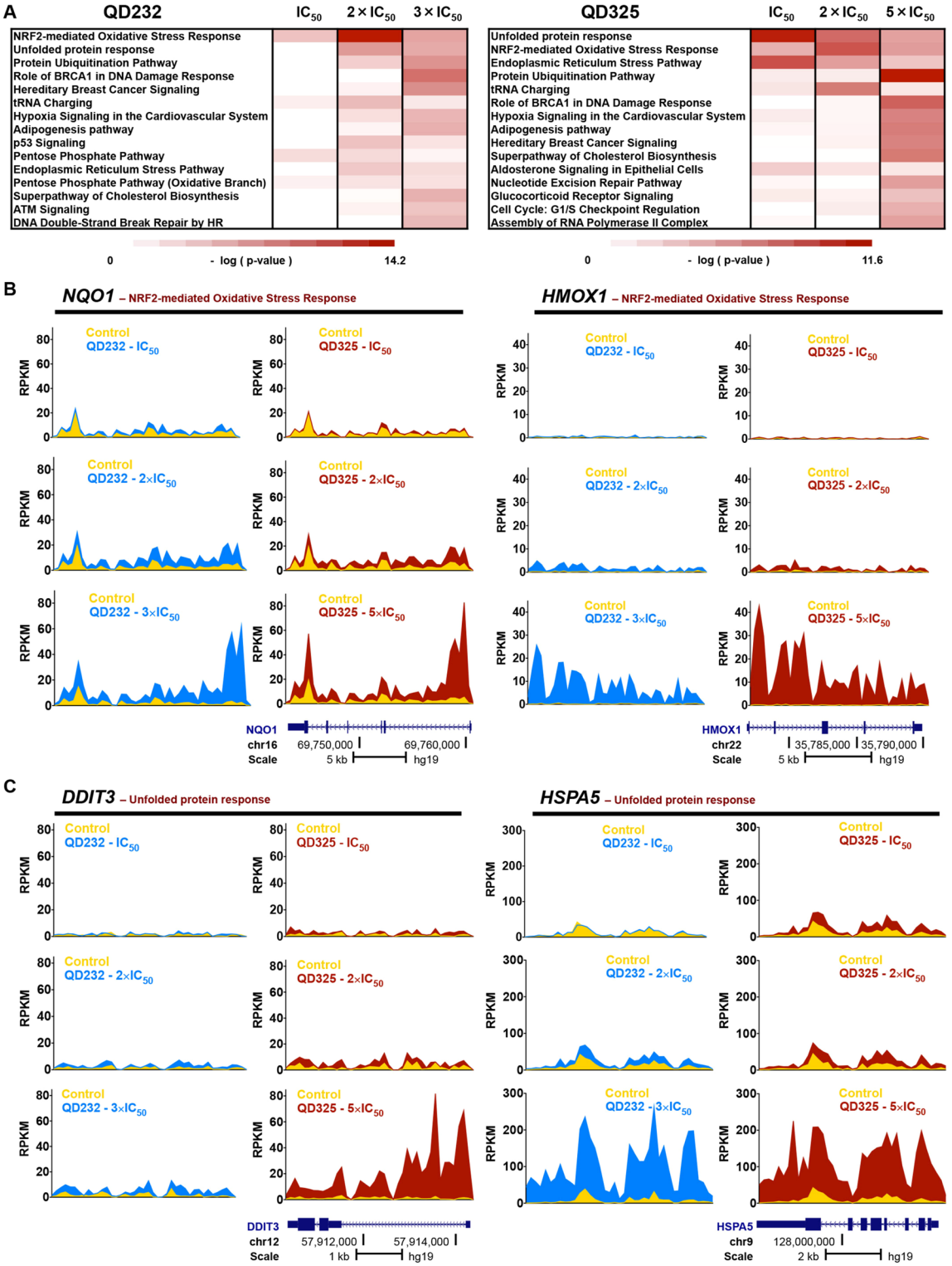

Figure 2. QD compounds induce oxidative stress and the unfolded protein response. (A) Top 15 canonical pathways induced by **QD232** or **QD325** treatment as revealed by IPA analysis of Bru-seq data. MIA PaCa-2 cells were treated with **QD232** (at 1, 2, or 3 times IC_{50}) or **QD325** (at 1, 2, or 5 times IC_{50}) for 4 h. Nascent RNA was labeled with 2 mM bromouridine during the last 30 min of treatment, immunocaptured, converted to cDNA libraries and deep sequenced. (B) Transcription of oxidative stress responsive genes *NQO1* and *HMOX1* was upregulated by **QD232** or **QD325** treatment in MIA PaCa-2 cells in a dose-dependent manner. (C) Transcription of unfolded protein response target genes *DDIT3* and *HSPA5* was upregulated by **QD232** or **QD325** treatment in MIA PaCa-2 cells.

and Sp4 in pancreatic cancer cells;[55−57] however, we did not observe selective downregulation of these transcription factor genes in our Bru-seq studies and these factors were not in our top 100 affected genes.

QD Compounds Inhibit Transcription of mtDNA from the D-Loop. Mitochondria play an important role in regulating redox homeostasis in mammalian cells. Deregulation of the expression of mitochondrial genes can lead to interruption of the oxidative

DOI: 10.1021/acs.jmedchem.7b01463
J. Med. Chem. 2018, 61, 1576−1594

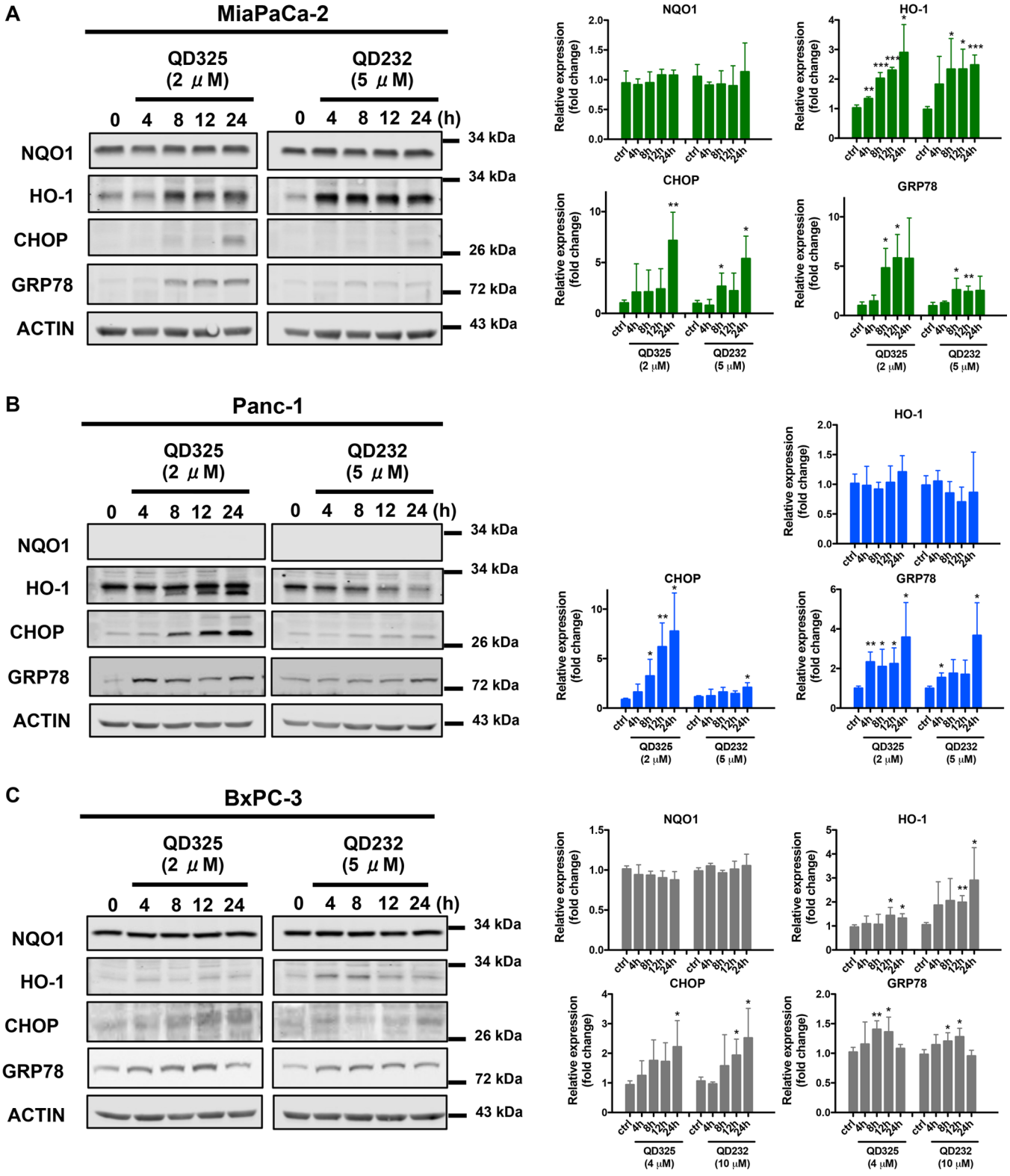

Figure 3. QD compounds induce protein expression of target genes for oxidative stress and unfolded protein response. Expression levels of oxidative stress responsive proteins NQO1, HO-1, and unfolded protein response target proteins CHOP and GRP78 were regulated to different extents by **QD232** or **QD325** treatment time dependently in (A) MIA PaCa-2, (B) Panc-1, and (C) BxPC-3 cells. Protein levels were quantified by ImageJ and normalized to respective loading controls. Data on quantification plots represent mean ± SD from three independent experiments. p values were calculated using student's t test. *, $p < 0.05$; **, $p < 0.01$, ***, $p < 0.001$.

phosphorylation pathway, resulting in the accumulation of ROS. Mitochondrial DNA (mtDNA) harbors 13 genes that encode proteins with important functions in the electron transport chain. The double-stranded circular mitochondrial genome comprises the guanine-rich heavy strand and the cytidine-rich light strand. Using Bru-seq, we observed significant inhibition of mtDNA transcription after a 4-h treatment with QD compounds at higher concentrations (Figure 4A; Figure S7). Both compounds

DOI: 10.1021/acs.jmedchem.7b01463
J. Med. Chem. 2018, 61, 1576−1594

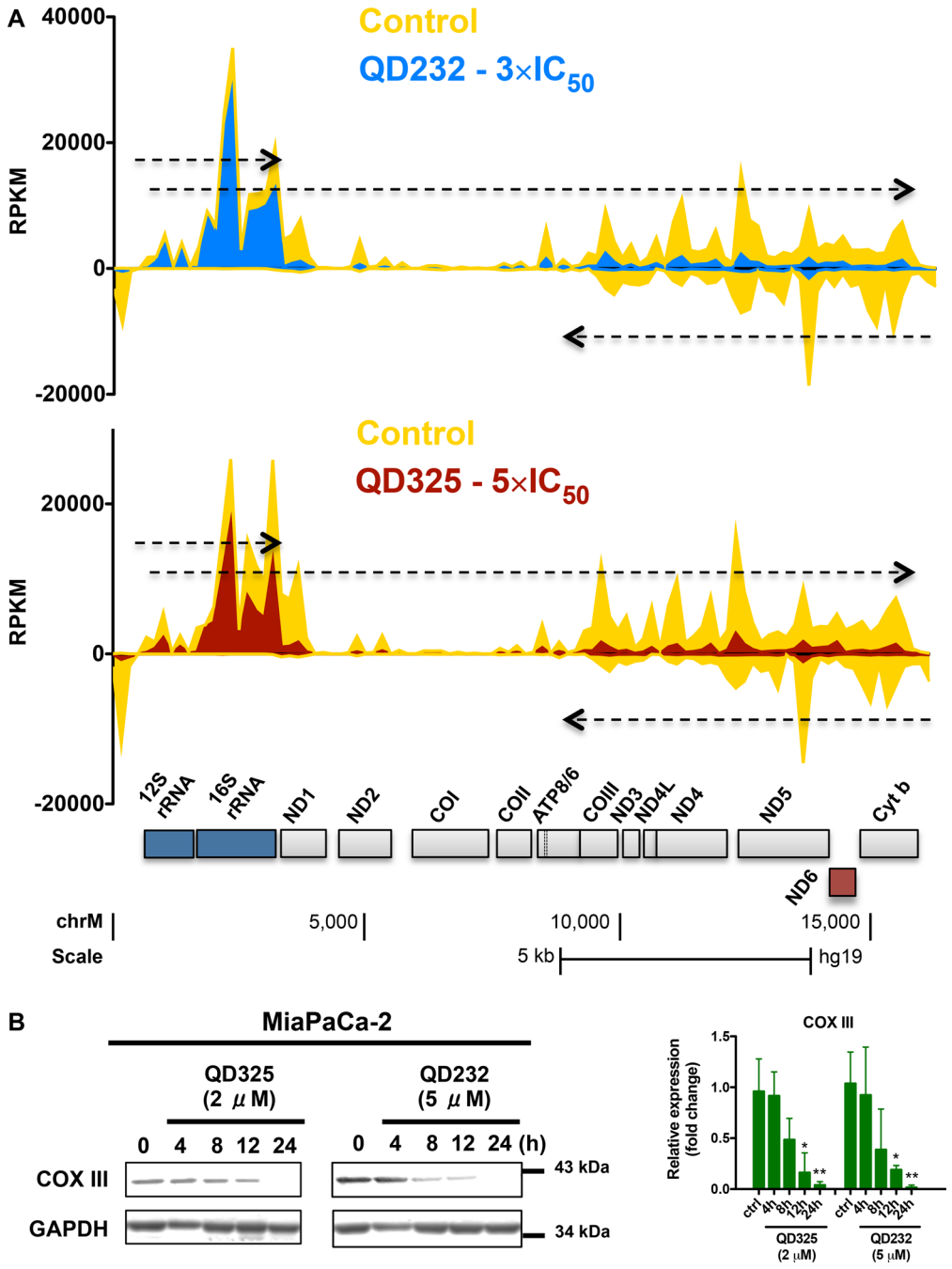

Figure 4. QD compounds show selective inhibition of transcription from the mitochondrial genome. (A) Nascent mitochondrial RNA synthesis was inhibited following a 4-h treatment with **QD232** (at 6.9 μM) or **QD325** (at 5.0 μM) in MIA PaCa-2 cells. Top forward arrows represent transcripts from the heavy strand. While the shorter arrow represents the shorter rRNA transcript regulated by the HSP1 promoter, the longer arrow represents transcript regulated by the HSP2 promoter that covers the full length of the heavy strand of the mitochondrial genome. Bottom reverse arrow represents the light strand transcript regulated by the LSP promoter. Transcription signals from DMSO-treated control cells are shown in yellow, while transcription signals from the **QD232**-treated cells are shown in blue, and signals from the **QD325**-treated cells are shown in red. The full-length transcripts from both heavy and light strands are further processed into functional tRNA, rRNA and mRNA molecules, whose corresponding genes are shown at the bottom of the panel. (B) Protein (COXIII) expression levels of the mitochondrial gene *COIII* were decreased by treatment of the QD compounds in MIA PaCa-2 cells. Protein levels were quantified by ImageJ and normalized to respective loading controls. Data on quantification plots represent mean ± SD from three independent experiments. p values were calculated using student's t test. *, $p < 0.05$; **, $p < 0.01$.

decreased COX III protein levels, which correlated to a reduced rate of transcription of the gene (Figure 4B). These results strongly suggest that the QD compounds disrupt mitochondrial function.

The D-loop (displacement loop) is a noncoding area of the mtDNA genome composed of a short three-stranded structure required for the regulation of initiation of mtDNA replication and transcription. This region contains two promoters on the heavy strand HSP1 and HSP2, one on the light strand, LSP, and also the mtDNA replication origin O_H. The D-loop region has been reported to be frequently mutated in lung, hepatocellular, colorectal and cervical cancers[58−61] and these D-loop mutations are linked to a poor prognosis of the disease.[62,63]

Using Bru-seq, we found that the QD compounds inhibited the transcription of mtDNA from both the heavy strand promoter

DOI: 10.1021/acs.jmedchem.7b01463
J. Med. Chem. 2018, 61, 1576−1594

HSP2 (top long arrow in Figure 4A) and the light strand promoter LSP (bottom arrow), thus inhibiting the expression of mitochondrial genes that are essential for mitochondrial oxidative phosphorylation. However, the activity of the heavy strand promoter HSP1 (top short arrow, Figure 4A), which regulates transcription of 12s rRNA and 16s rRNA, was less affected by the QDs. This pattern of transcriptional inhibition was not observed following treatments with UV light, camptothecin, or with 40 FDA-approved and other novel drugs developed in our laboratory (data not shown). Thus, the Bru-seq data showing selective transcriptional inhibition of the mitochondrial genome suggest that this mechanism may be linked to the toxicity induced by the **QD232** and **QD325** compounds.

QD325 Delays Tumor Growth without Systemic Toxicity. In NOD/SCID mice, MIA PaCa-2-derived xenograft showed significantly delayed growth following treatment with **QD325** (5 mg/kg). On day 44, the xenografts treated with **QD325** had only reached a size of 308 ± 72 mm^3 (p = 2.1E6) compared to 1291 ± 168 mm^3 for the xenografts in the control group (Figure 5A).

No symptoms of gross toxicity such as weakness, weight loss, or lethargy were observed in any treatment group for the duration of the treatments (Figure 5B). H&E-stained organ sections did not reveal any major histopathological changes, further confirming the *in vivo* tolerability of **QD325** (Figure 5C). Following the 44-day treatment, two mice from each group were used to

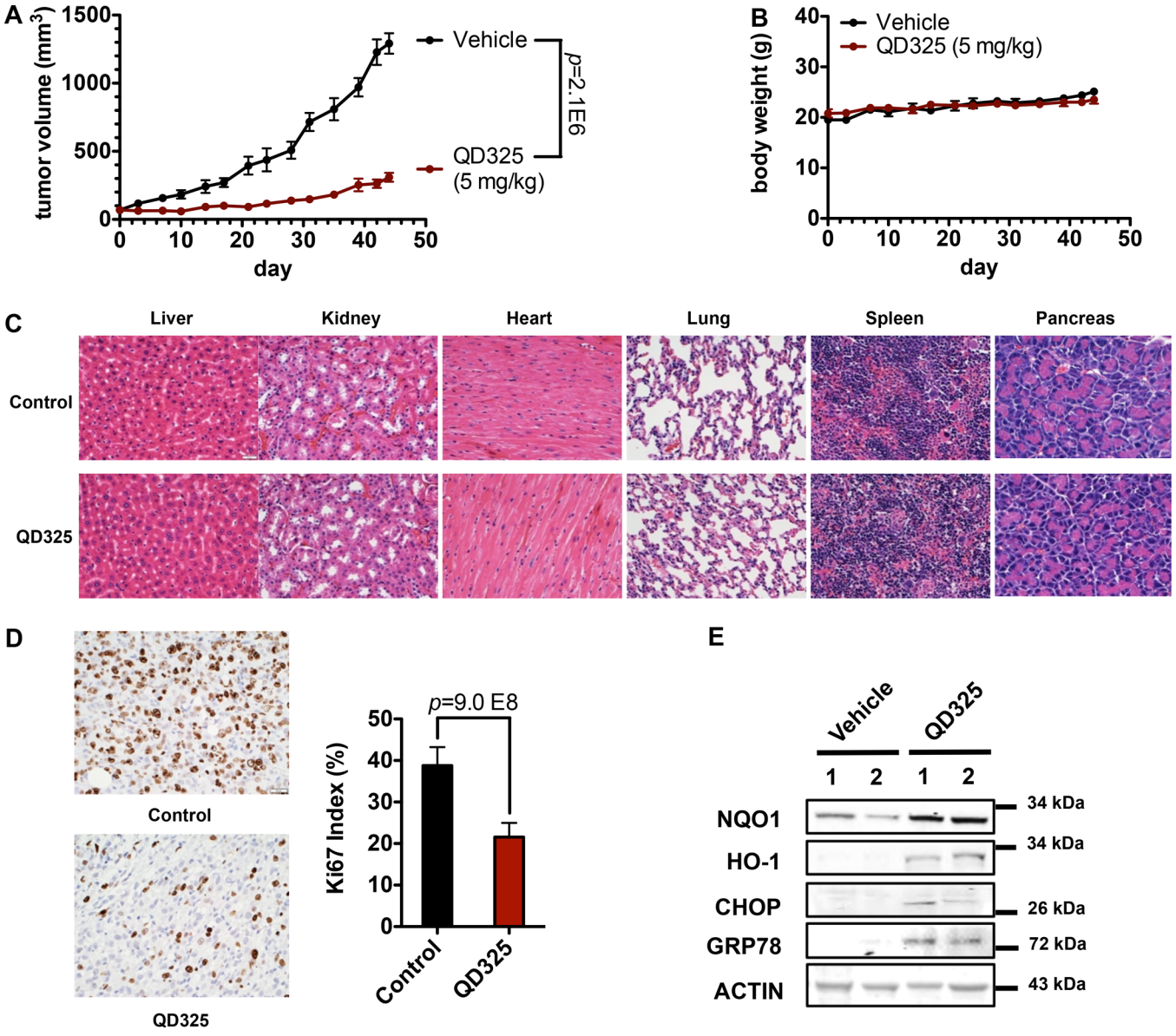

Figure 5. QD325 inhibits tumor growth of MIA PaCa-2 xenograft without systemic toxicity. (A) MIA PaCa-2 engrafted NOD/SCID mice were randomized into vehicle control (n = 5) or **QD325** treatment (n = 5) group when tumor size reached 65 mm^3. **QD325** was given at 5 mg/kg five times a week until day 44. (B) Body weight of engrafted mice was not affected by **QD325** treatment at 5 mg/kg five times a week until day 44. Data points represent mean ± SEM. (C) Representative micrographs of hematoxylin and eosin (H&E)-stained organ sections. Images were taken with an Olympus IX83 inverted microscope at 20× magnification. Histopathology inspection showed no major microscopic changes in major organs after **QD325** treatment at 5 mg/kg five times a week until day 44. (D) Representative immunohistochemistry images for Ki67 staining of MIA PaCa-2 xenograft sections. **QD325** decreased Ki67 index (percentage of Ki67 positive cells in the field) of treated tumors. Data represents mean ± SD (n = 9, 3 tumors from each group, 3 images of each tumor section). p values were calculated using student's t test. (E) NQO1, HO-1, CHOP, GRP78 protein levels in vehicle or **QD325**-treated MIA PaCa-2 xenografts.

DOI: 10.1021/acs.jmedchem.7b01463
J. Med. Chem. 2018, 61, 1576−1594

evaluate efficacy and safety of **QD325** at higher doses. While tumors in the control group exhibited rapid growth, **QD325** treatment was able to delay growth of the tumors without any overt systemic toxicity observed even at doses as high as 20 mg/kg (Figure 6A,B).

In line with the tumor growth inhibition, **QD325** treatment decreased the staining for the proliferation marker Ki67 in tumor tissues, suggesting inhibition of cell proliferation (Figure 5D). To further evaluate the mechanisms of action of **QD325** *in vivo*, we examined the protein levels of stress response markers in tumor lysates. NQO1, HO-1, CHOP, and GRP78 protein levels were significantly upregulated in **QD325**-treated tumors compared with tumors treated with vehicle, further confirming induction of oxidative stress and UPR as major mechanisms of action for **QD325** in these pancreatic cancer models (Figure 5E).

Gemcitabine is currently used as the standard of care for treatment of pancreatic cancer patients. Unfortunately, inherent or acquired resistance to gemcitabine represents a major challenge for successful treatment of this disease. Here we sought to explore the potential efficacy of administering **QD325** in combination with gemcitabine. In mice studies, gemcitabine is usually given at high doses (40−160 mg/kg) twice weekly. Considering its low tolerance in NOD/SCID mice, we compared antitumor activity of two different gemcitabine treatment schedules in a MIA PaCa-2 xenograft model in this mouse strain: (1) 15 mg/kg once a week for 48 days; (2) 15 mg/kg twice a week for the first 15 days. Similar antitumor activity was achieved by either schedule (Figure 6C). In both cases, gemcitabine was well tolerated and no weight loss was observed (Figure 6D). Therefore, schedule 1 was used for comparison of efficacy with **QD325** at 5 mg/kg and the combination of gemcitabine and **QD325**. **QD325** was given at 5 mg/kg five times a week and gemcitabine was given at 15 mg/kg once a week (Figure 6E). At the end of the 48-day treatment period, average tumor size was 1503 ± 189 mm^3 for the control group, 387 ± 74 mm^3 (p = 0.0049) for the gemcitabine group, 248 ± 72 mm^3 (p = 0.0030) for the **QD325** group, and 163 ± 83 mm^3 (p = 0.0023) for the combination of gemcitabine and **QD325** group (Figure 6E). Single agent treatment with **QD325** at 5 mg/kg showed similar antitumor activity as gemcitabine. In this experiment, both gemcitabine and **QD325** greatly inhibited tumor

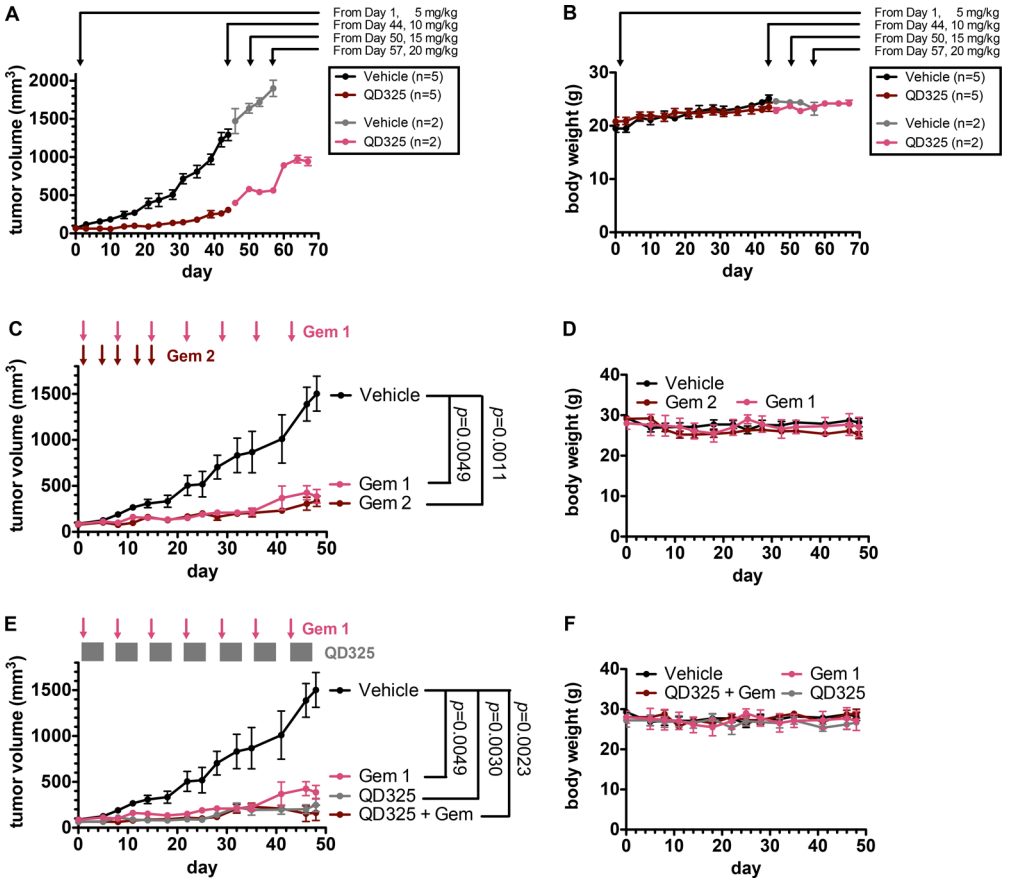

Figure 6. QD325 inhibits tumor growth of MIA PaCa-2 xenograft. (A) **QD325** treatment at 5 mg/kg inhibits growth of MIA PaCa-2 xenograft in NOD/SCID mice. MIA PaCa-2 engrafted mice were randomized into vehicle control (n = 5) or **QD325** treatment (n = 5) group when tumor size reached 65 mm^3. **QD325** was given at 5 mg/kg five times a week until day 44. Three mice from each group were euthanized for tissue analysis. Two mice remained in each group after day 44 and **QD325** dose was increased from 5 mg/kg to 20 mg/kg until day 67. (B) Body weight of engrafted mice was not affected by **QD325** treatment from 5 to 20 mg/kg. Error bars indicate mean ± SEM. (C) Gemcitabine treatment at 15 mg/kg inhibits growth of MIA PaCa-2 xenograft in NOD/SCID mice. MIA PaCa-2 engrafted mice were randomized into vehicle control (n = 4), gemcitabine treatment 1 (n = 3), gemcitabine treatment 2 (n = 4) groups when tumor size reached 75 mm^3. In treatment 1, gemcitabine was given at 15 mg/kg once a week for 48 days; in treatment 2, gemcitabine was given at 15 mg/kg twice a week for 15 days. Data points represent mean ± SEM. (D) Body weight of engrafted mice is not affected by gemcitabine treatment in either dosing frequency. (E) **QD325** treatment at 5 mg/kg inhibits growth of MIA PaCa-2 xenograft in NOD/SCID mice. MIA PaCa-2 engrafted mice were randomized into vehicle control (n = 4), gemcitabine treatment (n = 3), **QD325** treatment (n = 3) and combination treatment groups (n = 3) when tumor size reached 75 mm^3. **QD325** was given at 5 mg/kg five times a week and gemcitabine was given at 15 mg/kg once a week. Data points represent mean ± SEM. (F) Body weight of engrafted mice was not affected by gemcitabine or **QD325** treatment.

DOI: 10.1021/acs.jmedchem.7b01463
J. Med. Chem. 2018, 61, 1576−1594

growth as single agents. Importantly, the combination was well tolerated. and no weight loss was observed in any of the treatment groups, suggesting a reasonable safety profile of the drug combination (Figure 6F).

DISCUSSION

Altered redox homeostasis has been observed in various types of cancers including PDAC. ROS levels are increased as a result of elevated energy demands in cancer cells. To adapt to changes in the microenvironment, cancer cells hijack the intracellular antioxidant machinery to reach a new redox state that can facilitate their proliferation. Such dependency on an altered redox state provides novel therapeutic opportunities. Previously, we provided proof of concept that generation of additional ROS using the tool compound **QD232** can lead to the selective killing of cancer cells when they are challenged beyond their antioxidant capacity.[29,30] In order to expand upon our previous observations and to select a compound for future clinical development, we performed a lead optimization campaign and identified **QD325**, which showed a stronger induction of ROS and more potent cytotoxicity in PDAC cells (Figure 1).

As revealed by nascent RNA Bru-seq analysis, the NRF2-mediated oxidative stress response is induced within 4 h of treatment with the QD compounds (Figure 2). The cytoprotective NRF2 signaling pathway has been found to be cancer preventive under certain circumstances but oncogenic under other conditions.[64,65] Activating mutations in NRF2 and KEAP1 are often seen in cancers as an adaptation to elevated intrinsic ROS levels.[66] In PDAC, where such mutations are not very common, the redox state alteration can be supported through other pathways. The $Kras^{G12D}$ mutation found in >90% of PDAC cases, activates the Nrf2 signaling through the MAPK pathway, thus modifying the antioxidant program of PDAC cells to promote tumor progression.[22] This subtle balance is crucial for cancer cells as knockdown of NRF2 in PDAC cell lines results in decreased cell viability,[67] showing dependency of cell proliferation on the antioxidant pathway.

The NRF2 inhibitor, trig, can significantly sensitize PDAC cells to etoposide or TRAIL-induced apoptosis, and also enhances the antitumor response to etoposide in xenograft models.[68] However, trig was not cytotoxic as a single agent, and the sensitization of cells was dependent on the proteasome degradation pathway. An alternative strategy to target the altered redox balance in cancer cells would be to trigger ROS accumulation. ROS inducing-agents such as **QD232**,[30] piperlongumine,[69] and imexon[70] have shown single agent antitumor activities in pancreatic cancer models. Induction of ROS by the QD compounds alters this delicate balance and cells respond by upregulating the NRF2 pathway in an effort to counter the insult. However, excessive ROS overwhelms the system to the point of no return leading to cell death. A phase I trial of imexon and gemcitabine in patients with advanced pancreatic cancer demonstrated feasibility and antitumor responses[71] encouraging clinical testing of more potent compounds such as **QD325**. These results support the notion that manipulating redox homeostasis by inducing ROS could be an efficacious therapeutic strategy.

Another significant pathway upregulated following 4 h of QD treatment is the unfolded protein response (UPR) (Figure 2). In the ER, where an oxidizing environment is required for formation of disulfide bonds, the luminal redox state is under stringent regulation. UPR is triggered when there is imbalance between protein-folding demands and protein folding capacity, as well as any homeostatic perturbation that can cause protein misfolding, such as nutrition deprivation or redox insults.[72] Furthermore, UPR serves as a sensitive cytoprotective response to integrated stresses including oxidative stress. The activation of the NRF2-mediated oxidative stress response and UPR both imply that **QD232** and **QD325** treatments induce oxidative stress. While the activation of NRF2 protects cells against ROS, activation of UPR is considered to be both an adaptive response and a major executor of cell death in response to oxidative stress. UPR regulates cell survival on the basis of the severity and the duration of the ER stress. The proapoptotic path of UPR is adopted through several mechanisms including induction of CHOP and its transcription targets to activate apoptosis.[72] Upregulation of CHOP is observed following treatment with the QD compounds (Figure 3), suggesting that ER-mediated apoptosis is a major mechanism of cytotoxicity of the QD compounds.

For the mitochondrial genome, we observed substantial inhibition of transcription from the HSP2 and LSP promoters (Figure 4), with only modest change in the transcription from the HSP1 promoter (Figure S6). This suggests selectivity in QD-mediated inhibition of transcription. The displacement loop (D-loop) is a noncoding control region in the mitochondrial genome where promoters for transcription of the H and L strands (HSP and LSP), as well as the origin of replication (O_H) are located.[73] There are two promoters for the H-strand, while transcripts from HSP1 terminates right after the two rRNAs, transcripts from HSP2 cover the full strand and are subjected to subsequent processing into individual mRNA, tRNA and rRNA molecules.[74,75] The selective transcriptional inhibition of two out of the three promoters implies that mechanisms other than universal oxidative damaging contribute to such suppressed transcription, and might serve as a pharmacologically induced model to further elucidate regulation of transcription from the mitochondrial genome. We hypothesize that blockage of transcription initiation of selective promoters in the D-loop is a unique feature of the mechanism of action of the QD compounds.

In our *in vivo* xenograft model for pancreatic cancer, **QD325** showed substantial antitumor efficacy with a favorable safety profile. Our original lead compound **QD232** significantly delayed tumor growth at 20 mg/kg in a similar MIA PaCa-2 xenograft model as reported earlier,[29] suppressing growth of tumor by 65% in the 31-day study. **QD325**, the most potent compound in this lead optimization campaign, showed improved potency by achieving comparable tumor inhibitory effect at a dose of only 5 mg/kg. **QD325** did not show any toxicity following repetitive treatments with doses as high as 20 mg/kg, suggesting that it is well tolerated and that it has a favorable therapeutic window. We repeated the experiments with two independent experiments under the same conditions (Figure 5A and Figure 6E), and observed similar results (76% vs 83% inhibition of tumor growth) for **QD325**-treated animals.

Gemcitabine is the standard of care treatment for pancreatic cancer patients. In our studies, **QD325** showed similar antitumor effect as gemcitabine, supporting the application of **QD325** as a novel therapeutic option with a distinct new mechanism, especially for patients with gemcitabine resistance. Due to its remarkable ROS-induction in tumor cells, we expect **QD325** to be less toxic than gemcitabine. In general, drug combinations demonstrate survival advantages over single-agent therapy as long as they have manageable safety profiles. Our studies show that combination with gemcitabine is tolerable without additional toxicity burden to mice. However, to perform clinically relevant synergy studies, both drugs need to be evaluated at optimal doses and in additional cell lines and mice models. These findings warrant the

DOI: 10.1021/acs.jmedchem.7b01463
J. Med. Chem. 2018, 61, 1576−1594

development of **QD325** as a novel treatment for PDAC as a single agent and in combination with standard of care drugs.

CONCLUSIONS

In this study, we successfully optimized the anticancer ROS modulator **QD232**, leading to the discovery of **QD325** that shows significant ROS dependent anticancer activity in PDAC models. Bru-seq analysis predicted cellular responses in the nucleus, ER, and mitochondrial for the ROS-mediated cytotoxicity in pancreatic cancer cells, providing in-depth understanding of the unique mechanisms of this active class of anticancer compounds. Significant antitumor efficacy and the favorable safety profile of **QD325** in vivo provides strong rationale for further developing these QD drugs to target mitochondria as a novel approach to treat PDAC.

EXPERIMENTAL SECTION

Chemistry. *General Methods.* The reference compound **QD232** and the intermediate **6** were prepared as previously described by us (see refs 30 and 32, respectively). All solvents, including anhydrous solvents, and chemicals were purchased from Aldrich Co., Alfa Aesar, or Carlo Erba and were used without further purification. All reactions involving air- or moisture-sensitive compounds were performed under a nitrogen atmosphere using oven-dried glassware and syringes to transfer solutions. Analytical thin-layer chromatography (TLC) was carried out on Merck silica gel F-254 plates. Flash chromatography purifications were performed on Merck Silica gel 60 (230−400 mesh ASTM) as a stationary phase. Melting points (mp) were determined using an Electrothermal melting point or a Köfler apparatus and are uncorrected. Nuclear magnetic resonance (^{1}H NMR, ^{13}C NMR) spectra were recorded in $CDCl_3$ or DMSO-d_6 on 400 MHz Bruker Avance III. Chemical shifts (δ) are reported in parts per million (ppm) downfield from tetramethylsilane (TMS), used as an internal standard. Splitting patterns are designated as follow: s, singlet; d, doublet; t, triplet; q, quadruplet; m, multiplet; brs, broad singlet; dd, double doublet. The assignment of exchangeable protons (OH and NH) was confirmed by the addition of D_2O. Mass spectra were obtained on a Hewlett-Packard 5989 mass engine spectrometer, or a MALDI micro MX (Waters, Micromass) equipped with a reflectron analyzer. Elemental analyses were performed on a PerkinElmer Elemental Analyzer 2400-CHN at Laboratory of Microanalysis, Department of Chemistry and Pharmacy, University of Sassari (Italy), and were within ±0.4% of the theoretical values (Table S8), thus confirming ≥95% purity.

*General Method A: Preparation of Compounds **QD324−327**, **329**, **331**, **332**, **334−336**, **338**, **353−357**.* A solution of quinazoline-5, 8-dione, cerium(III) chloride heptahydrate ($CeCl_3{\cdot}7\ H_2O$, 1.1 equiv) and (3,4,5)-substituted aniline (1.1 equiv) in absolute ethanol was stirred at room temperature for 1−2 h. Next, most of the ethanol was removed under vacuum, and water was added, followed by the extraction with CH_2Cl_2. The organic layers were washed with water and brine, dried over anhydrous Na_2SO_4, and concentrated to dryness. Then, the crude product was purified by flash chromatography to give the expected product.

*General Method B: Preparation of the Compounds **QD328**, **330**, **333**, **337**.* A solution of quinazoline-5,8-dione, cerium(III) chloride heptahydrate ($CeCl_3{\cdot}7\ H_2O$, 1.1 equiv) and (3,4,5)-substituted aniline (1.1 equiv) in absolute ethanol was stirred at room temperature for 2−6 h. Next, most of the ethanol was removed under vacuum, and water was added, followed by the extraction with CH_2Cl_2. The organic layers were dried over sodium sulfate (Na_2SO_4) and concentrated to dryness. Then, the crude residue was treated with water, and the solid residue that precipitated was filtered and triturated with petroleum ether to give the desired product.

*3,6-Dimethoxy-2-nitrobenzaldehyde (**2**).* Nitric acid (8.0 mL; 179.02 mmol), acetic anhydride (8.0 mL, 84.24 mmol), and 2, 5-dimethoxybenzaldehyde (**1**, 4.0 g, 24.07 mmol) were added at 0 °C with stirring, respectively. After 1.5 h of stirring, the mixture was poured onto 20 mL ice/water. The resultant yellow solid was filtered, washed with cold water, and then purified by flash chromatography on silica gel using ethyl acetate-petroleum ether (1:1) to give first the regioisomer 2,5-dimethoxy-4-nitrobenzaldehyde, and then (by further elution with only ethyl acetate) the desired compound **2**. Yield: 68%. R_f = 0.10 (ethyl acetate-petroleum ether 5:5); mp: 167 °C. ^{1}H NMR 400 MHz (DMSO-d_6): δ 10.25 (s, 1H), 7.70 (d, 1H), 7.48 (d, 1H), 3.95 (s, 3H), 3.86 (s, 3H). ^{1}H NMR 400 MHz ($CDCl_3$): δ 10.39 (s, 1H), 7.30 (d, 1H), 7.12 (d, 1H), 3.97 (s, 3H), 3.89 (s, 3H). MS: m/z 211 $[M]^+$.

*N,N′-[(3,6-Dimethoxy-2-nitrophenyl)methanediyl]diformamide (**3**).* A solution of 3,6-dimethoxy-2-nitrobenzaldehyde (**2**, 11.90 g, 56.35 mmol) in formamide (66.5 eq., 150 mL), heated at 40 °C, was exposed to dry HCl gas (1 h) until the temperature reached 80 °C. Then, the solution was cooled to room temperature, and water/ice was added. Pale yellow colored precipitate was formed, which was filtered, dried and triturated with ethyl acetate and petroleum ether to yield the desired compound. Yield: 90%. R_f = 0.26 (dichloromethane-methanol 9.5:0.5); mp: 255 °C. ^{1}H NMR 400 MHz (DMSO-d_6): δ 8.67 (d, 2H), 7.92 (s, 2H), 7.28 (s, 2H), 6.77 (t, 1H), 3.88 (s, 3H), 3.82 (s, 3H). MS: m/z 283 $[M^+]$.

*5,8-Dimethoxyquinazoline (**4**).* Zinc powder (22.9 g) was added to a suspension of *N,N′*-[(3,6-dimethoxy-2-nitrophenyl)methanediyl)]-diformamide (**3**, 7.0 g, 24.71 mmol) in triturated ice (92 g) and glacial acetic acid (32 mL), under constant magnetic stirring. The reaction mixture was stirred for 2 h in an ice bath and for 4 h at room temperature. After filtration of the reaction mixture through filter paper, the resulting solution was dropped on cooled 50% NaOH (120 mL), and the yellow colored suspension thus formed was left without stirring for 1 h. Next, the suspension was filtered and the solid dried (at 30−40 °C) to give a yellow powder. The solid was then solubilized in ethyl acetate, filtered, dried over anhydrous Na_2SO_4, and concentrated to dryness yielding the desired compound. Yield: 79%. R_f = 0.46 (dichloromethane-methanol 9.5:0.5); mp: 106 °C. ^{1}H NMR 400 MHz (DMSO-d_6): δ 9.64 (s, 1H), 9.28 (s, 1H), 7.39 (d, 1H), 7.10 (d, 1H), 3.98 (s, 3H), 3.94 (s, 3H). MS: m/z 190 $[M]^+$

*(3-Aminopropyl)triphenylphosphonium bromide hydrobromide (**6**).* To a 50 mL round-bottom flask equipped with a magnetic stirring bar, triphenylphosphine (1.0 eq., 1.0 g, 3.82 mmol), 3-bromopropylamine hydrobromide (**5**, 1.0 eq., 0.84 g, 3.82 mmol), and acetonitrile (7 mL), were added. The resulting suspension was heated to reflux, and the mixture was stirred for 16 h. The reaction was cooled to room temperature, then *n*-hexane was added, and the resulting solid was filtered, washed with *n*-hexane, dissolved in 100 mL isopropanol and precipitated with cold diethyl ether, to give a white powder. Yield: 50%; R_f = 0.28 (dichlorometane-methanol 9:1); mp: 200 °C. ^{1}H NMR 400 MHz ($CDCl_3$): δ 7.95−7.92 (m, 3H), 7.84−7.74 (m, 15 H), 3.74 (m, 2H), 3.00−2.98 (m, 2H), 1.85 (m, 2H).

*Quinazoline-5,8-dione (**QD323**).* A solution of 5,8-dimethoxyquinazoline (**4**, 0.35 g, 1.84 mmol) in (7:3) acetonitrile:water (10 mL) was cooled at 0 °C in an ice bath, and a solution of ceric ammonium nitrate (2.7 eq., 2.72 g, 4.97 mmol) in (9:1) acetonitrile:water (10 mL) was added dropwise. The reaction mixture was stirred for 20 min, then poured into ice/water and extracted (8−10 times) with CH_2Cl_2. The organic layer was washed (5−6 times) with water, dried over anhydrous Na_2SO_4 and concentrated to dryness to give a brown powder. Yield: 69%. R_f = 0.62 (dichloromethane-methanol 9.5:0.5); mp: > 320 °C. ^{1}H NMR 400 MHz (DMSO-d_6): δ 9.69 (s, 1H), 9.43 (s, 1H), 7.28 (d, 1H), 7.18 (d, 1H). ^{13}C NMR 400 MHz (DMSO-d_6): δ 184.07, 182.88, 162.08, 156.27, 152.61, 139.46, 137.74, 124.61. MS: m/z 160 $[M]^+$

*6-((4-Phenoxyphenyl)amino)quinazoline-5,8-dione (**QD324**).* The reaction mixture consisted of quinazoline-5,8-dione (**QD323**, 0.10 g, 0.62 mmol), cerium(III) chloride heptahydrate ($CeCl_3{\cdot}7\ H_2O$, 1.1 eq., 0.26 g, 0.69 mmol), 4-phenoxyaniline (1.1 eq., 0.13 g, 0.69 mmol), and absolute ethanol (11 mL). Flash chromatography (ethyl acetate-petroleum ether 6:4) gave compound **QD324** as a violet powder. Yield: 65%. R_f = 0.30 (ethyl acetate-petroleum ether 6:4); mp: 169−171 °C. ^{1}H NMR 400 MHz ($CDCl_3$): δ 9.66 (s, 1H), 9.49 (s, 1H), 7.51 (s, 1H), 7.39 (t, 2H), 7.25 (d, 2H), 7.20−7.15 (m, 1H), 7.09−7.04 (m, 4H), 6.53 (s, 1H). ^{13}C NMR 400 MHz ($CDCl_3$): δ 180.65, 180.39, 163.76, 156.48, 156.31, 154.40, 145.15, 130.90, 130.01, 125.25, 124.04, 123.34, 119.76, 119.28, 104.65. MS: m/z 343 $[M]^+$

DOI: 10.1021/acs.jmedchem.7b01463
J. Med. Chem. 2018, 61, 1576−1594

*6-([1,1′-Biphenyl]-4-ylamino)quinazoline-5,8-dione (**QD325**).* The reaction mixture consisted of quinazoline-5,8-dione (**QD323**, 0.16 g, 1.01 mmol), cerium(III) chloride heptahydrate ($CeCl_3 \cdot 7\ H_2O$, 1.1 eq., 0.41 g, 1.11 mmol), 4-aminobiphenyl (1.1 eq., 0.19 g, 1.11 mmol), and absolute ethanol (19 mL). Flash chromatography (ethyl acetate-petroleum ether 7:3) gave compound **QD325** as a violet powder. Yield: 58%. R_f = 0.48 (ethyl acetate-petroleum ether 8:2); mp: 230 °C. ^{1}H NMR 400 MHz ($CDCl_3$): δ 9.68 (s, 1H), 9.51 (s, 1H), 7.68 (d, 2H), 7.65 (s, 1H), 7.60 (d, 2H), 7.48 (t, 2H), 7.42−7.36 (m, 3H), 6.73 (s, 1H). ^{13}C NMR 400 MHz ($CDCl_3$): δ 180.67, 180.52, 163.78, 156.39, 154.32, 144.33, 139.71, 135.44, 128.99, 128.53, 127.53, 127.00, 123.26, 105.20. MS: m/z 327 $[M]^+$

*6-((3,4,5-Trimethoxyphenyl)amino)quinazoline-5,8-dione (**QD326**).* The reaction mixture consisted of quinazoline-5,8-dione (**QD323**, 0.07 g, 0.44 mmol), cerium(III) chloride heptahydrate ($CeCl_3 \cdot 7\ H_2O$, 1.1 eq., 0.18 g, 0.48 mmol), 3,4,5-trimethoxyaniline (1.1 eq., 0.09 g, 0.48 mmol), and absolute ethanol (8 mL). Flash chromatography (ethyl acetate-petroleum ether from 7:3 to 8:2) gave compound **QD326** as a violet powder. Yield: 88%. R_f = 0.18 (ethyl acetate-petroleum ether 8:2); mp: 161−162 °C. ^{1}H NMR 400 MHz ($CDCl_3$): δ 9.67 (s, 1H), 9.49 (s, 1H), 7.51 (s, 1H), 6.59 (s, 1H), 6.50 (s, 2H), 3.88 (s, 9H). ^{13}C NMR 400 MHz ($CDCl_3$): δ 180.61, 180.40, 163.77, 156.33, 154.15, 144.90, 136.96, 131.87, 123.30, 105.00, 101.20, 61.07, 56.39. MS: m/z 341 $[M]^+$

*6-((4-(Trifluoromethoxy)phenyl)amino)quinazoline-5,8-dione (**QD327**).* The reaction mixture consisted of quinazoline-5,8-dione (**QD323**, 0.05 g, 0.31 mmol), cerium(III) chloride heptahydrate ($CeCl_3 \cdot 7\ H_2O$, 1.1 eq., 0.13 g, 0.34 mmol), 4-(trifluoromethoxy)aniline (1.1 eq., 0.046 mL, 0.34 mmol), and absolute ethanol (6 mL). Flash chromatography (dichloromethane-methanol 9.7:0.3) gave compound **QD327** as a dark red powder. Yield: 67%. R_f = 0.53 (dichloromethane-methanol 9.5:0.5); mp: 114 °C. ^{1}H NMR 400 MHz ($CDCl_3$): δ 9.68 (s, 1H), 9.51 (s, 1H), 7.55 (s, 1H), 7.33 (s, 4H), 6.58 (s, 1H). MS: m/z 335 $[M]^+$

*4-((5,8-Dioxo-5,8-dihydroquinazolin-6-yl)amino)benzenesulfonamide (**QD328**).* The reaction mixture consisted of quinazoline-5,8-dione (**QD323**, 0.05 g, 0.31 mmol), cerium(III) chloride heptahydrate ($CeCl_3 \cdot 7\ H_2O$, 1.1 eq., 0.13 g, 0.34 mmol), sulfanilamide (1.1 eq., 0.06 g, 0.34 mmol), and absolute ethanol (6 mL). The precipitate was filtered and triturated with petroleum ether gave compound **QD328** as a red powder. Yield: 59%. R_f = 0.16 (ethyl acetate-petroleum ether 8:2); mp: > 320 °C. ^{1}H NMR 400 MHz (DMSO-d_6): δ 9.72 (s, 1H), 9.64 (s, 1H), 9.44 (s, 1H), 7.88 (d, 2H), 7.60 (d, 2H), 7.38 (s, 2H), 6.46 (s, 1H). ^{13}C NMR 400 MHz (DMSO-d_6): δ 180.50, 180.32, 162.58, 155.78, 153.46, 145.33, 140.91, 140.20, 127.38, 127.05, 124.19, 123.17, 112.38, 105.11. MS: m/z 331 $[M+1]^+$

*6-((4-(Hydroxymethyl)phenyl)amino)quinazoline-5,8-dione (**QD329**).* The reaction mixture consisted of quinazoline-5,8-dione (**QD323**, 0.05 g, 0.31 mmol), cerium(III) chloride heptahydrate ($CeCl_3 \cdot 7\ H_2O$, 1.1 eq., 0.13 g, 0.34 mmol), 4-aminobenzyl alcohol (1.1 eq., 0.04 g, 0.34 mmol), and absolute ethanol (6 mL). Flash chromatography (dichloromethane-methanol 9.7:0.3) gave compound QD329 as a brown-red powder. Yield: 27%. R_f = 0.30 (dichloromethane-methanol 9.5:0.5); mp: 203 °C. ^{1}H NMR 400 MHz ($CDCl_3$): δ 9.67 (s, 1H), 9.50 (s, 1H), 7.59 (s, 1H), 7.47 (d, 2H), 7.29 (d, 2H), 6.64 (s, 1H), 4.75 (s, 2H). MS: m/z 303 $[M + Na]^+$

*4-((5,8-Dioxo-5,8-dihydroquinazolin-6-yl)amino)benzamide (**QD330**).* The reaction mixture consisted of quinazoline-5,8-dione (**QD323**, 0.05 g, 0.31 mmol), cerium(III) chloride heptahydrate ($CeCl_3 \cdot 7\ H_2O$, 1.1 eq., 0.13 g, 0.34 mmol), 4-aminobenzamide (1.1 eq., 0.05 g, 0.34 mmol), and absolute ethanol (6 mL). The precipitate was filtered and triturated with petroleum ether gave compound **QD330** as a brown powder. Yield: 24%. R_f = 0.58 (dichloromethane-methanol 9.5:0.5); mp: > 320 °C. ^{1}H NMR 400 MHz (DMSO-d_6): δ 9.65 (s, 1H), 9.63 (s, 1H), 9.43 (s, 1H), 7.95 (d, 2H), 7.49 (d, 2H), 7.38 (s, 2H), 6.42 (s, 1H). MS: m/z 295 $[M+1]^+$

*Methyl 4-((5,8-Dioxo-5,8-dihydroquinazolin-6-yl)amino)benzoate (**QD331**).* The reaction mixture consisted of quinazoline-5,8-dione (**QD323**, 0.06 g, 0.37 mmol), cerium(III) chloride heptahydrate ($CeCl_3 \cdot 7\ H_2O$, 1.1 eq., 0.15 g, 0.41 mmol), methyl 4-aminobenzoate (1.1 eq., 0.06 g, 0.41 mmol), and absolute ethanol (7.2 mL). Flash chromatography (ethyl acetate-petroleum ether from 6:4 to 7:3) gave compound **QD331** as a red powder. Yield: 42%. R_f = 0.35 (ethyl acetate-petroleum ether 7:3); mp: 226−230 °C. ^{1}H NMR 400 MHz ($CDCl_3$): δ 9.69 (s, 1H), 9.52 (s, 1H), 8.14 (d, 2H), 7.72 (s, 1H), 7.36 (d, 2H), 6.81 (s, 1H), 3.95 (s, 3H). ^{13}C NMR 400 MHz ($CDCl_3$): δ 180.75, 180.40, 165.96, 163.85, 156.57, 153.96, 143.34, 140.64, 131.51, 127.69, 123.27, 121.66, 121.55, 106.35, 52.35. MS: m/z 309 $[M]^+$

*Ethyl 4-((5,8-Dioxo-5,8-dihydroquinazolin-6-yl)amino)benzoate (**QD332**).* The reaction mixture consisted of quinazoline-5,8-dione (**QD323**, 0.13 g, 0.81 mmol), cerium(III) chloride heptahydrate ($CeCl_3 \cdot 7\ H_2O$, 1.1 eq., 0.33 g, 0.89 mmol), ethyl 4-aminobenzoate (1.1 eq., 0.15 g, 0.89 mmol), and absolute ethanol (16 mL). Flash chromatography (ethyl acetate-petroleum ether 6.5:3.5) gave compound **QD332** as a red powder. Yield: 39%. R_f = 0.36 (ethyl acetate-petroleum ether 7:3); mp: 206−207 °C. ^{1}H NMR 400 MHz ($CDCl_3$): δ 9.69 (s, 1H), 9.52 (s, 1H), 8.14 (d, 2H), 7.72 (s, 1H), 7.36 (d, 2H), 6.80 (s, 1H), 4.43−4.38 (q, 2H), 1.42 (t, 3H). ^{13}C NMR 400 MHz ($CDCl_3$): δ 180.74, 180.42, 165.49, 163.85, 156.56, 153.98, 143.38, 140.53, 131.47, 128.08, 123.27, 121.65, 106.31, 61.31, 14.34. MS: m/z 323 $[M]^+$

*(3-((5,8-Dioxo-5,8-dihydroquinazolin-6-yl)amino)phenyl)boronic acid (**QD333**).* The reaction mixture consisted of quinazoline-5,8-dione (**QD323**, 0.05 g, 0.31 mmol), cerium(III) chloride heptahydrate ($CeCl_3 \cdot 7\ H_2O$, 1.1 eq., 0.13 g, 0.34 mmol), 3-aminophenylboronic acid (1.1 eq., 0.05 g, 0.34 mmol), and absolute ethanol (6 mL). The precipitate was filtered and triturated with petroleum ether gave compound **QD333** as a red powder. Yield: 48%. R_f = 0.37 (dichloromethane-methanol 9.5:0.5); mp: 208−210 °C. ^{1}H NMR 400 MHz (DMSO-d_6): δ 9.61 (s, 1H), 9.52 (s, 1H), 9.41 (s, 1H), 8.20 (s, 2H), 7.77−7.70 (m, 2H), 7.43 (m, 2H), 6.23 (s, 1H). MS: m/z 318 $[M + Na]^+$

*6-((4′-Fluoro-[1,1′-biphenyl]-4-yl)amino)quinazoline-5,8-dione (**QD334**).* The reaction mixture consisted of quinazoline-5,8-dione (**QD323**, 0.05 g, 0.31 mmol), cerium(III) chloride heptahydrate ($CeCl_3 \cdot 7\ H_2O$, 1.1 eq., 0.13 g, 0.34 mmol), 4-amino-4′-fluorobiphenyl (1.1 eq., 0.06 g, 0.34 mmol), and absolute ethanol (6 mL). Flash chromatography (ethyl acetate-petroleum ether from 7:3 to 8:2) gave compound **QD334** as a violet powder. Yield: 29%. R_f = 0.32 (ethyl acetate-petroleum ether 7:3); mp: 285−289 °C. ^{1}H NMR 400 MHz ($CDCl_3$): δ 9.68 (s, 1H), 9.51 (s, 1H), 7.63 (d, 2H), 7.55 (t, 2H), 7.53 (s, 1H), 7.37 (d, 2H), 7.16 (t, 2H), 6.72 (s, 1H). ^{13}C NMR 400 MHz ($CDCl_3$): δ 180.64, 180.53, 163.97, 163.79, 161.51, 156.39, 154.30, 144.33, 138.70, 135.98, 135.47, 128.65, 128.39, 123.33, 116.03, 115.82, 105.21. MS: m/z 345 $[M]^+$

*6-((4′-Ethyl-[1,1′-biphenyl]-4-yl)amino)quinazoline-5,8-dione (**QD335**).* The reaction mixture consisted of quinazoline-5,8-dione (**QD323**, 0.05 g, 0.34 mmol), cerium(III) chloride heptahydrate ($CeCl_3 \cdot 7\ H_2O$, 1.1 eq., 0.14 g, 0.37 mmol), 4-amino-4′-ethylbiphenyl (1.1 eq., 0.07 g, 0.37 mmol), and absolute ethanol (6.5 mL). Flash chromatography (ethyl acetate-petroleum ether from 6:4 to 7:3) gave compound **QD335** as a red-violet powder. Yield: 60%. R_f = 0.36 (ethyl acetate-petroleum ether 7:3); mp: 232 °C. ^{1}H NMR 400 MHz ($CDCl_3$): δ 9.66 (s, 1H), 9.49 (s, 1H), 7.68 (s, 1H), 7.66 (d, 2H), 7.51 (d, 2H), 7.34 (d, 2H), 7.30 (d, 2H), 6.71 (s, 1H), 2.74−2.68 (q, 2H), 1.29 (t, 3H). ^{13}C NMR 400 MHz ($CDCl_3$): δ 180.67, 180.48, 163.73, 156.35, 154.34, 144.35, 144.09, 139.64, 137.03, 135.15, 128.53, 128.46, 126.89, 123.35, 123.24, 105.11, 28.54, 15.55. MS: m/z 356 $[M+1]^+$

*6-((4′-Methoxy[1,1′-biphenyl]-4-yl)amino)quinazoline-5,8-dione (**QD336**).* The reaction mixture consisted of quinazoline-5,8-dione (**QD323**, 0.05 g, 0.34 mmol), cerium(III) chloride heptahydrate ($CeCl_3 \cdot 7\ H_2O$, 1.1 eq., 0.14 g, 0.37 mmol), 4′-methoxy-biphenyl-4-ylamine (1.1 eq., 0.07 g, 0.37 mmol), and absolute ethanol (6.5 mL). Flash chromatography (ethyl acetate-petroleum ether from 7:3 to 10:0) gave compound **QD336** as a dark violet powder. Yield: 69%. R_f = 0.29 (ethyl acetate-petroleum ether 7:3); mp: 270−272 °C. ^{1}H NMR 400 MHz ($CDCl_3$): δ 9.67 (s, 1H), 9.51 (s, 1H), 7.63 (d, 2H), 7.61 (s, 1H), 7.53 (d, 2H), 7.32 (d, 2H), 7.01 (d, 2H), 6.71 (s, 1H), 3.87 (s, 3H). ^{13}C NMR 400 MHz ($CDCl_3$): δ 180.67, 180.47, 163.77, 159.58, 156.36, 154.37, 144.38, 139.38, 134.81, 132.20, 128.05, 128.01, 123.29, 123.19, 114.44, 105.09, 55.40. MS: m/z 357 $[M]^+$

*6-((4′-Amino-[1,1′-biphenyl]-4-yl)amino)quinazoline-5,8-dione (**QD337**).* The reaction mixture consisted of quinazoline-5,8-dione (**QD323**, 0.05 g, 0.34 mmol), cerium(III) chloride heptahydrate ($CeCl_3 \cdot 7\ H_2O$, 1.1 eq., 0.14 g, 0.37 mmol), benzidine (1.1 eq., 0.07 g, 0.37 mmol),

DOI: 10.1021/acs.jmedchem.7b01463
J. Med. Chem. 2018, 61, 1576−1594

and absolute ethanol (6.5 mL). The precipitate was filtered and triturated with petroleum ether gave compound **QD337** as a dark violet powder. Yield: 16%. R_f = 0.71 (dichlorometane-methanol 9.5:0.5); mp: > 320 °C. ^{1}H NMR 400 MHz (DMSO-d_6): δ 9.66 (s, 1H), 9.63 (s, 1H), 9.44 (s, 1H), 7.83 (d, 2H), 7.64 (d, 1H), 7.53 (d, 2H), 7.40 (d, 2H), 6.65 (d, 1H), 6.40 (s, 1H), 5.27 (s, 2H). MS: m/z 342 $[M]^+$

*6-((2-Fluoro-4′-methyl-[1,1′-biphenyl]-4-yl)amino)quinazoline-5,8-dione (**QD338**).* The reaction mixture consisted of quinazoline-5,8-dione (**QD323**, 0.06 g, 0.35 mmol), cerium(III) chloride heptahydrate ($CeCl_3$·7 H_2O, 1.1 eq., 0.14 g, 0.38 mmol), 2-fluoro-4′-methyl-biphenyl-4-ylamine (1.1 eq., 0.08 g, 0.38 mmol), and absolute ethanol (6.7 mL). Flash chromatography (ethyl acetate-petroleum ether, from 6:4 to 8:2) gave compound **QD338** as a violet powder. Yield: 60%. R_f = 0.26 (ethyl acetate-petroleum ether 7:3); mp: 282−283 °C. ^{1}H NMR 400 MHz ($CDCl_3$): δ 9.69 (s, 1H), 9.52 (s, 1H), 7.62 (s, 1H), 7.52 (t, 1H), 7.45 (d, 2H), 7.29 (d, 2H), 7.14 (t, 2H), 6.75 (s, 1H), 2.42 (s, 3H). ^{13}C NMR 400 MHz ($CDCl_3$): δ 180.61, 180.47, 163.83, 156.49, 143.93, 138.14, 131.79, 129.40, 128.89, 128.71, 123.31, 118.67, 110.85, 110.58, 105.75, 21.24. MS: m/z 359 $[M]^+$

*(3-(4-Aminobenzamido)propyl)triphenylphosphonium bromide (**QD339**).* To a solution of 4-aminobenzoic acid (1.0 eq., 0.076 g, 0.55 mmol) in CH_2Cl_2 (12 mL), *N,N*-diisopropylethylamine (DIPEA, 5 eq 0.48 mL, 2.75 mmol), and HBtU (1.0 eq., 0.206 g, 0.55 mmol) were added. The reaction mixture was stirred for 15 min, and (3-aminopropyl)-triphenylphosphonium bromide (**6**, 3 eq 0.80 g, 1.66 mmol) and DMAP (0.04 eq., 2.7 μg, 0.02 mmol) were added. The resulting mixture was stirred at room temperature for 5 h, filtered, washed with CH_2Cl_2, and concentrated to dryness. The crude product was purified by flash chromatography on silica gel using dichloromethane-isopropanol (9.5:0.5) to give **QD339** as a beige powder. Yield: 70%; R_f = 0.27 (dichlorometane-methanol 9:1); mp: 203−205 °C. ^{1}H NMR 400 MHz ($CDCl_3$): δ 8.91 (t, 1H), 8.10 (d, 2H), 7.77−7.72 (m, 9H), 7.61−7.58 (m, 6H), 6.70 (d, 2H), 3.94−3.90 (m, 2H), 3.72−3.71 (m, 2H), 1.95 (m, 2H). MS: m/z 439.

*(3-(4-((5,8-Dioxo-5,8-dihydroquinazolin-6-yl)amino)benzamido)-propyl) triphenylphosphonium bromide (**QD340**).* A solution of quinazoline-5,8-dione (**5**, 1.0 eq., 0.04 g, 0.25 mmol), cerium(III) chloride heptahydrate ($CeCl_3$·7 H_2O, 1.1 eq., 0.102 g, 0.27 mmol) and (3-(4-aminobenzamido)propyl)triphenylphosphonium bromide (**QD339**, 1.1 eq., 0.143 g, 0.27 mmol) in absolute ethanol (5 mL) was stirred at room temperature for 2 h. Then, most of the ethanol was removed under vacuum, and water was added, followed by the extraction with CH_2Cl_2. The organic layers were washed with water, brine, dried over anhydrous sodium sulfate, and concentrated to dryness. The crude product was triturated with petroleum ether to give **QD340** as a red powder. Yield: 42%; R_f = 0.45 (dichlorometane-methanol 9:1); mp: 205 °C. ^{1}H NMR 400 MHz ($CDCl_3$): δ 9.90 (t, 1H), 9.67 (s, 1H), 9.50 (s, 1H), 8.46 (d, 2H), 7.79−7.72 (m, 10H), 7.65−7.62 (m, 6H), 7.37 (d, 2H), 6.74 (s, 1H), 3.97−3.93 (m, 2H), 3.75−3.74 (m, 2H), 2.00 (m, 2H). MS: m/z 597.

*6-((3-Methoxyphenyl)amino)quinazoline-5,8-dione (**QD353**).* The reaction mixture consisted of quinazoline-5,8-dione (**QD323**, 0.05 g, 0.31 mmol), cerium(III) chloride heptahydrate ($CeCl_3$·7 H_2O, 1.1 eq., 0.13 g, 0.34 mmol), *m*-anisidine (1.1 eq., 0.38 mL, 0.34 mmol), and absolute ethanol (6 mL). Flash chromatography (ethyl acetate-petroleum ether 6:4) gave compound **QD353** as a dark violet powder. Yield: 43%. R_f = 0.30 (ethyl acetate-petroleum ether 7:3); mp: 142 °C. ^{1}H NMR 400 MHz ($CDCl_3$): δ 9.67 (s, 1H), 9.50 (s, 1H), 7.56 (s, 1H), 7.36 (t, 1H), 6.88 (d, 2H), 6.83 (d, 2H), 6.82 (s, 1H), 6.69 (s, 1H), 3.84 (s, 3H). ^{13}C NMR 400 MHz ($CDCl_3$): δ 180.65, 180.56, 163.76, 160.81, 156.36, 154.28, 144.45, 137.40, 130.75, 123.33, 115.25, 112.07, 109.17, 105.34, 55,53. MS: m/z 281 $[M]^+$

*6-((4-Methoxyphenyl)amino)quinazoline-5,8-dione (**QD354**).* The reaction mixture consisted of quinazoline-5,8-dione (**QD323**, 0.06 g, 0.37 mmol), cerium(III) chloride heptahydrate ($CeCl_3$·7 H_2O, 1.1 eq., 0.15 g, 0.41 mmol), *p*-anisidine (1.1 eq., 0.05 g, 0.41 mmol), and absolute ethanol (7.2 mL). Flash chromatography (ethyl acetate-petroleum ether from 6.5:3.5 to 8:2) gave compound **QD354** as a dark powder. Yield: 41%. R_f = 0.32 (ethyl acetate-petroleum ether 7:3); mp: 238 °C. ^{1}H NMR 400 MHz ($CDCl_3$): δ 9.66 (s, 1H), 9.48 (s, 1H), 7.49 (s, 1H), 7.21 (d, 2H), 6.98 (d, 2H), 6.48 (s, 1H), 3.85 (s, 3H). ^{13}C NMR 400 MHz ($CDCl_3$): δ 180.76, 180.28, 163.73, 156.24, 154.52, 145.34, 128.75, 125.18, 123.36, 115.16, 104.34, 55,62. MS: m/z 281 $[M]^+$

*6-((3,4-Dimethoxyphenyl)amino)quinazoline-5,8-dione (**QD355**).* The reaction mixture consisted of quinazoline-5,8-dione (**QD323**, 0.06 g, 0.40 mmol), cerium(III) chloride heptahydrate ($CeCl_3$·7 H_2O, 1.1 eq., 0.16 g, 0.44 mmol), 3,4-dimethoxyaniline (1.1 eq., 0.067 g, 0.44 mmol), and absolute ethanol (7.6 mL). Flash chromatography (ethyl acetate-petroleum ether from 7:3 to 10:0) gave compound **QD355** as a dark powder. Yield: 70%. R_f = 0.23 (ethyl acetate-petroleum ether 8:2); mp: 241−242 °C. ^{1}H NMR 400 MHz ($CDCl_3$): δ 9.66 (s, 1H), 9.49 (s, 1H), 7.50 (s, 1H), 6.92 (d, 2H), 6.86 (d, 2H), 6.78 (s, 1H), 6.53 (s, 1H), 3.92 (s, 3H), 3.90 (s, 3H). ^{13}C NMR 400 MHz ($CDCl_3$): δ 180.73, 180.31, 163.75, 156.75, 156.26, 154.48, 149.97, 148.10, 145.21, 129.02, 123.34, 116.10, 111.74, 107.50, 104.54, 56,18. MS: m/z 334 $[M + Na]^+$

*6-((4-Fluorobenzyl)amino)quinazoline-5,8-dione (**QD356**).* The reaction mixture consisted of quinazoline-5,8-dione (**QD323**, 0.06 g, 0.40 mmol), cerium(III) chloride heptahydrate ($CeCl_3$·7 H_2O, 1.1 eq., 0.16 g, 0.44 mmol), 4-fluorobenzylamine (1.1 eq., 0.05 mL, 0.44 mmol), and absolute ethanol (7.6 mL). Flash chromatography (ethyl acetate-petroleum ether from 7:3 to 8:2) gave compound **QD356** as an orange powder. Yield: 35%. R_f = 0.30 (ethyl acetate-petroleum ether 8:2); mp: 203 °C. ^{1}H NMR 400 MHz ($CDCl_3$): δ 9.64 (s, 1H), 9.43 (s, 1H), 7.30 (t, 2H), 7.09 (t, 2H), 6.28 (s, 1H), 6.05 (s, 1H), 4.40 (d, 2H). ^{13}C NMR 400 MHz ($CDCl_3$): δ 180.33, 179.62, 163.93, 163.67, 161.47, 156.16, 154.57, 146.96, 130.68, 129.43, 123.35, 116.14, 103.76, 46.30. MS: m/z 283 $[M]^+$

*6-((3,5-Dimethoxyphenyl)amino)quinazoline-5,8-dione (**QD357**).* The reaction mixture consisted of quinazoline-5,8-dione (**QD323**, 0.06 g, 0.40 mmol), cerium(III) chloride heptahydrate ($CeCl_3$·7 H_2O, 1.1 eq., 0.16 g, 0.44 mmol), 3,5-dimethoxyaniline (1.0 eq., 0.07 g, 0.44 mmol), and absolute ethanol (7.6 mL). Flash chromatography (ethyl acetate-petroleum ether from 6:4 to 7:3) gave compound **QD357** as a violet powder. Yield: 70%. R_f = 0.45 (ethyl acetate-petroleum ether 8:2); mp: 204−206 °C. ^{1}H NMR 400 MHz (DMSO-d_6): δ 9.66 (s, 1H), 9.43 (s, 1H), 7.05 (s, 1H), 5.97 (s, 2H), 5.72 (s, 2H), 3.62 (s, 6H). ^{13}C NMR 400 MHz ($CDCl_3$): δ 183.14, 182.27, 162.43, 159.30, 157.54, 152.64, 150.43, 145.40, 138.54, 125.32, 100.99, 91.24, 55,74. MS: m/z 312 $[M+1]^+$\

*(3-(3-Aminobenzamido)propyl)triphenylphosphonium bromide (**QD358**).* To a solution of 3-aminobenzoic acid (1.0 eq., 0.076 g, 0.55 mmol) in CH_2Cl_2 (12 mL), *N,N*-diisopropylethylamine (DIPEA, 5 eq 0.48 mL, 2.75 mmol), and HBtU (1.0 eq., 0.206 g, 0.55 mmol) were added. The reaction mixture was stirred for 15 min before (3-aminopropyl)triphenylphosphonium bromide (**6**, 3 eq., 0.80 g, 1.66 mmol) and DMAP (0.04 eq., 2.7 μg, 0.02 mmol) were added. The resulting mixture was stirred at room temperature for 5 h, filtered, washed with CH_2Cl_2, and concentrated to dryness. The crude product was purified by flash chromatography on silica gel using dichloromethane-isopropanol (9.5:0.5) to give an orange powder. Yield: 59%; R_f = 0.45 (dichlorometane-methanol 9:1); mp: 223 °C. ^{1}H NMR 400 MHz ($CDCl_3$): δ 8.97 (t, 1H), 7.77−7.73 (m, 10H), 7.62−7.60 (m, 6H), 7.55 (d, 1H), 7.21 (t, 1H), 6.78 (d, 1H), 3.92−3.88 (m, 2H), 3.73−3.72 (m, 2H), 1.97 (m, 2H). MS: m/z 439.

*(3-(3-((5,8-Dioxo-5,8-dihydroquinazolin-6-yl)amino)benzamido)-propyl) triphenylphosphonium bromide (**QD359**).* A solution of quinazoline-5,8-dione (1.0 eq., 0.04 g, 0.25 mmol), cerium(III) chloride heptahydrate ($CeCl_3$·7 H_2O, 1.1 eq., 0.102 g, 0.27 mmol) and (3-(3-aminobenzamido)propyl)triphenyl phosphonium bromide (**QD358**, 1.0 eq., 0.130 g, 0.25 mmol) in absolute ethanol (5 mL) was stirred at room temperature for 1.5 h. Then, most of the ethanol was removed under vacuum, and water was added, followed by the extraction with CH_2Cl_2. The organic layers were washed with water, dried over anhydrous sodium sulfate and concentrated to dryness. The crude product was purified by flash chromatography on silica gel using dichloromethane-methanol (9.4:0.4) to give a red powder. Yield: 30%; R_f = 0.21 (dichlorometane-methanol 9:1); mp: 108−110 °C. ^{1}H NMR 400 MHz ($CDCl_3$): δ 9.78 (t, 1H), 9.64 (s, 1H), 9.47 (s, 1H), 8.34 (d, 2H), 8.19 (d, 2H), 7.77−7.73 (m, 10H), 7.64−7.62 (m, 6H), 7.54 (t, 1H), 7.45 (d, 1H), 6.63 (s, 1H), 3.92−3.88 (m, 2H), 3.74−3.73 (m, 2H), 2.05−2.00 (m, 2H). MS: m/z 597.

Biology. Cell Culture. MIA PaCa-2, Panc-1 and BxPC-3 pancreatic cancer cell lines were obtained from the ATCC. Normal pancreatic cells

DOI: 10.1021/acs.jmedchem.7b01463
J. Med. Chem. 2018, 61, 1576−1594

HPDE and HPNE were kindly provided by Dr. Diane Simeone (Translational Oncology Program, University of Michigan, Ann Arbor, MI). Gemcitabine resistant cell line MIA PaCa-2-GR (gemcitabine resistant) was kindly provided by Dr. Sarkar (Department of Pathology, Wayne State University, Detroit, MI) All cell lines were cultured as monolayer and maintained in RPMI1640 supplemented with 10% fetal bovine serum (FBS) in a humidified atmosphere with 5% CO_2 at 37 °C. MIA PaCa-2-GR culture was supplemented with 200 nM gemcitabine.

MTT Assay. Cytotoxicity of compounds was evaluated with 3-(4, 5-dimethylthiazol-2-yl)-2,5-diphenyltetrazolium bromide (MTT) assay. Cells were placed in 96-well plate at 3000−8000 cells/well. After the cells were allowed to attach overnight, compounds were added to the wells at sequential dilutions (30 nM−10 μM for most cell lines). After 72 h of treatment, MTT was added into the media to a final concentration of 300 μg/mL. Cells were incubated for 3 h at 37 °C, and the insoluble formazan converted by viable cells were dissolved in 150 μL of DMSO. Absorbance at 570 nm was read by microplate reader (Molecular devices, Sunnyvale, CA), and inhibition of cell proliferation was calculated using the following formula: Inhibition of cell proliferation (%) = $(1 - OD_{treatment}/OD_{control}) \times 100\%$

ROS Detection Assay. Cells were detached by 0.05% trypsin-EDTA, neutralized, centrifuged (1200 rpm, 5 min) and resuspended in cell culture media. Suspension were then treated with 20 μM cell permeable H2DCFDA for 30 min at 37 °C. Cells were then centrifuged (1200 rpm, 5 min) and washed with cell culture media to remove excess probe. After the cells were washed, they were placed in black-wall 384-well plate at 20 000 cells/well, incubated for 30 min, and treated by compounds at designated conditions. Fluorescent signal were then read at 493 nm/523 nm on BioTek H1 plate reader for ROS detection.

Bru-seq Analysis for Nascent RNA Synthesis. Bru-seq analysis was performed as previously reported.[36] Briefly, 4×10^6 MIA PaCa-2 cells were placed in 10 cm dishes on Day 1. On Day 2, cells were treated with DMSO, **QD232** or **QD325** for 4 h. Bromouridine was added into the media to label newly synthesized nascent RNA during the last 30 min of treatment to a final concentration of 2 mM. Cells were then collected in TRIZOL, and total RNA was isolated. Bromouridine-containing RNA was immunocaptured from total RNA, converted into cDNA libraries and deep sequenced at the University of Michigan Sequencing Core. Sequencing reads were mapped to the HG19 reference genome. Preranked gene lists were generated for each treatment through ranking genes by fold changes in RNA synthesis levels compared with control, and analyzed with GSEA (Broad Institute, MA)[76,77]

Western Blotting. Cells (4×10^5) were cultured in 60 mm tissue dishes and treated with QD compounds at designated concentrations. After treatment, cells were lysed with cell lysis buffer at 4 °C for 30 min and centrifuged (12000 rpm, 10 min, 4 °C). Protein concentrations of supernatants were measured with BCA assay (Thermo Fisher Scientific). Next, 40 μg protein per sample was subjected to SDS-PAGE analysis. Proteins were then electrotransferred to methanol activated immobilon-FL PVDF membranes (EMD Millipore, Billerica, MA). Membranes were blocked with 5% skim milk in TBST buffer and incubated with primary antibodies (anti-NQO1, anti-HO-1, anti-CHOP, and anti-GAPDH from Cell Signaling, anti-COXIII, anti-ACTIN and anti-GRP78 from Santa Cruz Biotechnology) 1:1000 dilutions overnight at 4 °C. Membranes were then washed with TBST (10 min × 3), incubated with Dylight 800-conjugated secondary antibodies (Thermo Fisher Scientific, Rockford, IL) 1:5000 dilutions in 5% milk for 1 h at room temperature, and washed with TBST (10 min × 2) and TBS (10 min). The fluorescent signal was then scanned by Odyssey Imaging Systems (LI-COR Biosciences, Lincoln, NE).

Xenograft Studies. MIA PaCa-2 cells (2.0×10^6) in a 100 μL suspension of RPMI1640 was injected subcutaneously into dorsal flank of 6-week NOD/SCID mice. Tumor size was monitored twice a week through caliper measurement using the following equation: $V = d^2 \times D/2$, where d represents width and D represents length of the tumor. In study 1, mice were randomly grouped ($n = 5$ per group) when average tumor size reached 65 mm^3. Daily treatment was given at 5 days on 2 days off cycles. **QD325** was given at 5 mg/kg in 100 μL vehicle (5% DMSO, 60% Propylene glycol, 35% Saline) by intraperitoneal injection. Study was concluded on Day 44 when average tumor size in the group reached 1200 mm^3. An unpaired t test was performed for data analysis, and $p < 0.05$ was considered significant. For a tolerance test, two mice remained on each group beyond day 44, and **QD325** dose was gradually increased to 20 mg/kg until day 67. Procedures for study 2 with gemcitabine treatment are detailed in Supporting Information.

Histochemical Analysis. At the time of necropsy, tumors, hearts, kidneys, livers, lungs, spleens and pancreases were collected, fixed in 10% neutral buffered formalin, embedded in paraffin, and sectioned. Sections (5 μM) were stained with hematoxylin and eosin to facilitate histologic examination. For Ki67 expression level, immunohistochemistry staining was performed on sections with Ki67 antibody. Embedding, sectioning and staining of samples were performed by ULAM pathology core for animal research at the University of Michigan. Representative images were taken on Olympus IX83 microscope with 20× magnification.

■ ASSOCIATED CONTENT

Supporting Information

The Supporting Information is available free of charge on the ACS Publications website at DOI: 10.1021/acs.jmedchem.7b01463.

Correlation of cytotoxicity of QD compounds and ROS induction (Figure S2); list of top 30 canonical pathways affected by QD compound treatments (Figures S3 and S4); list of top 50 gene sets up regulated by QD compound treatments (Figure S5); list of top 50 gene sets down regulated by QD compound treatments (Figure S6); panels showing **QD232** or **QD325** treatment that selectively inhibits synthesis of mtDNA transcripts (Figure S7); and elemental analyses for tested compounds (Table S8) PDF)

Additional compound data (CSV)

■ AUTHOR INFORMATION

Corresponding Authors

*M.S. Phone: +39 079-228-753. Fax: +39 079-229-559. E-mail: mario.sechi@uniss.it.

*N.N. Phone: 734-647-2732. Fax: 734-763-8152. E-mail: neamati@umich.edu.

ORCID

Mario Sechi: 0000-0003-2983-6090

Nouri Neamati: 0000-0003-3291-7131

Notes

The authors declare the following competing financial interest(s): Certain aspects of the reported compounds are included in patent applications.

■ ACKNOWLEDGMENTS

This work was supported by NIH grant R01 CA188252 and a grant from the University of Michigan Forbes Institute for Cancer Discovery. M.S. gratefully acknowledges the Regione Autonoma della Sardegna (within the frame of Legge regionale n. 7/2007), and the Fondazione Banco di Sardegna for its partial support.

■ ABBREVIATIONS USED

Bru-seq, bromouridine labeled RNA sequencing; D-loop, displacement loop; DMAP, 4-dimethylaminopyridine; DIPEA, *N*,*N*-diisopropylethylamine; DMF, dimethylformamide; GSEA, Gene Set Enrichment Analysis; HSP, heavy strand promoter; LSP, light strand promoter; ROS, reactive oxygen species; HPLC, high-pressure liquid chromatography; HPDE, human pancreatic ductal epithelial; H2DCFDA, 2′,7′-Dichlorodihydrofluorescein diacetate; HBTU, (2-(1*H*-benzotriazol-1-yl)-1,1,3,3-tetramethyluronium hexafluorophosphate; IPA, ingenuity pathway analysis; IC50, half-maximum inhibitory concentration;

DOI: 10.1021/acs.jmedchem.7b01463
J. Med. Chem. 2018, 61, 1576−1594

MTT, 3-(4,5-dimethylthiazol-2-yl)-2,5-diphenyltetrazolium bromide; mtDNA, mitochondrial DNA; NAC, *N*-acetyl-cysteine; PBS, phosphate-buffered saline; PDAC, pancreatic ductal adenocarcinoma; QDs, quinazolinediones; UPR, unfolded protein response

REFERENCES

(1) Siegel, R. L.; Miller, K. D.; Jemal, A. Cancer statistics, 2017. *CA-Cancer J. Clin.* **2017**, *67*, 7−30.

(2) Sohal, D. P.; Mangu, P. B.; Khorana, A. A.; Shah, M. A.; Philip, P. A.; O'Reilly, E. M.; Uronis, H. E.; Ramanathan, R. K.; Crane, C. H.; Engebretson, A.; Ruggiero, J. T.; Copur, M. S.; Lau, M.; Urba, S.; Laheru, D. Metastatic pancreatic cancer: American Society of Clinical Oncology clinical practice guideline. *J. Clin. Oncol.* **2016**, *34*, 2784−2796.

(3) Ryan, D. P.; Hong, T. S.; Bardeesy, N. Pancreatic adenocarcinoma. *N. Engl. J. Med.* **2014**, *371*, 1039−1049.

(4) Von Hoff, D. D.; Ervin, T.; Arena, F. P.; Chiorean, E. G.; Infante, J.; Moore, M.; Seay, T.; Tjulandin, S. A.; Ma, W. W.; Saleh, M. N.; Harris, M.; Reni, M.; Dowden, S.; Laheru, D.; Bahary, N.; Ramanathan, R. K.; Tabernero, J.; Hidalgo, M.; Goldstein, D.; Van Cutsem, E.; Wei, X.; Iglesias, J.; Renschler, M. F. Increased survival in pancreatic cancer with nab-paclitaxel plus gemcitabine. *N. Engl. J. Med.* **2013**, *369*, 1691−1703.

(5) Conroy, T.; Desseigne, F.; Ychou, M.; Bouche, O.; Guimbaud, R.; Becouarn, Y.; Adenis, A.; Raoul, J. L.; Gourgou-Bourgade, S.; de la Fouchardiere, C.; Bennouna, J.; Bachet, J. B.; Khemissa-Akouz, F.; Pere-Verge, D.; Delbaldo, C.; Assenat, E.; Chauffert, B.; Michel, P.; Montoto-Grillot, C.; Ducreux, M. Groupe Tumeurs Digestives of, U.; Intergroup, P. FOLFIRINOX versus gemcitabine for metastatic pancreatic cancer. *N. Engl. J. Med.* **2011**, *364*, 1817−1825.

(6) Kamisawa, T.; Wood, L. D.; Itoi, T.; Takaori, K. Pancreatic cancer. *Lancet* **2016**, *388*, 73−85.

(7) Suker, M.; Beumer, B. R.; Sadot, E.; Marthey, L.; Faris, J. E.; Mellon, E. A.; El-Rayes, B. F.; Wang-Gillam, A.; Lacy, J.; Hosein, P. J.; Moorcraft, S. Y.; Conroy, T.; Hohla, F.; Allen, P.; Taieb, J.; Hong, T. S.; Shridhar, R.; Chau, I.; van Eijck, C. H.; Koerkamp, B. G. FOLFIRINOX for locally advanced pancreatic cancer: a systematic review and patient-level meta-analysis. *Lancet Oncol.* **2016**, *17*, 801−810.

(8) Conroy, T.; Bachet, J. B.; Ayav, A.; Huguet, F.; Lambert, A.; Caramella, C.; Marechal, R.; Van Laethem, J. L.; Ducreux, M. Current standards and new innovative approaches for treatment of pancreatic cancer. *Eur. J. Cancer* **2016**, *57*, 10−22.

(9) Fogel, E. L.; Shahda, S.; Sandrasegaran, K.; DeWitt, J.; Easler, J. J.; Agarwal, D. M.; Eagleson, M.; Zyromski, N. J.; House, M. G.; Ellsworth, S.; El Hajj, I.; O'Neil, B. H.; Nakeeb, A.; Sherman, S. A multidisciplinary approach to pancreas cancer in 2016: A review. *Am. J. Gastroenterol.* **2017**, *112*, 537−554.

(10) Falasca, M.; Kim, M.; Casari, I. Pancreatic cancer: Current research and future directions. *Biochim. Biophys. Acta, Rev. Cancer* **2016**, *1865*, 123−132.

(11) Mukherjee, I.; Powell, B.; Parianos, M.; Downs, D.; Ross, S. B. Available technologies and clinical applications of targeted chemotherapy in pancreatic cancer. *Cancer Genet.* **2016**, *209*, 582−591.

(12) Martinez-Useros, J.; Li, W.; Cabeza-Morales, M.; Garcia-Foncillas, J. Oxidative stress: A new target for pancreatic cancer prognosis and treatment. *J. Clin. Med.* **2017**, *6*, 29.

(13) Trachootham, D.; Alexandre, J.; Huang, P. Targeting cancer cells by ROS-mediated mechanisms: a radical therapeutic approach? *Nat. Rev. Drug Discovery* **2009**, *8*, 579−591.

(14) Moloney, J. N.; Cotter, T. G. ROS signalling in the biology of cancer. *Semin. Cell Dev. Biol.* **2017**. DOI: 10.1016/j.semcdb.2017.05.023. Published Online: June 3, 2017.

(15) Idelchik, M.; Begley, U.; Begley, T. J.; Melendez, J. A. Mitochondrial ROS control of cancer. *Semin. Cancer Biol.* **2017**, *47*, 57−66.

(16) Dharmaraja, A. T. Role of reactive oxygen species (ROS) in therapeutics and drug resistance in cancer and bacteria. *J. Med. Chem.* **2017**, *60*, 3221−3240.

(17) Panieri, E.; Santoro, M. M. ROS homeostasis and metabolism: a dangerous liason in cancer cells. *Cell Death Dis.* **2016**, *7*, e2253.

(18) Diebold, L.; Chandel, N. S. Mitochondrial ROS regulation of proliferating cells. *Free Radical Biol. Med.* **2016**, *100*, 86−93.

(19) Li, X.; Fang, P.; Mai, J.; Choi, E. T.; Wang, H.; Yang, X. F. Targeting mitochondrial reactive oxygen species as novel therapy for inflammatory diseases and cancers. *J. Hematol. Oncol.* **2013**, *6*, 19.

(20) Chio, I. I. C.; Tuveson, D. A. ROS in cancer: The burning question. *Trends Mol. Med.* **2017**, *23*, 411−429.

(21) Fruehauf, J. P.; Meyskens, F. L., Jr. Reactive oxygen species: a breath of life or death? *Clin. Cancer Res.* **2007**, *13*, 789−794.

(22) DeNicola, G. M.; Karreth, F. A.; Humpton, T. J.; Gopinathan, A.; Wei, C.; Frese, K.; Mangal, D.; Yu, K. H.; Yeo, C. J.; Calhoun, E. S.; Scrimieri, F.; Winter, J. M.; Hruban, R. H.; Iacobuzio-Donahue, C.; Kern, S. E.; Blair, I. A.; Tuveson, D. A. Oncogene-induced Nrf2 transcription promotes ROS detoxification and tumorigenesis. *Nature* **2011**, *475*, 106−109.

(23) Kong, B.; Qia, C.; Erkan, M.; Kleeff, J.; Michalski, C. W. Overview on how oncogenic Kras promotes pancreatic carcinogenesis by inducing low intracellular ROS levels. *Front. Physiol.* **2013**, *4*, 246.

(24) Storz, P. KRas, ROS and the initiation of pancreatic cancer. *Small GTPases* **2017**, *8*, 38−42.

(25) Zhang, L.; Li, J.; Ma, J.; Chen, X.; Chen, K.; Jiang, Z.; Zong, L.; Yu, S.; Li, X.; Xu, Q.; Lei, J.; Duan, W.; Li, W.; Shan, T.; Ma, Q.; Shen, X. The relevance of Nrf2 pathway and autophagy in pancreatic cancer cells upon stimulation of reactive oxygen species. *Oxid. Med. Cell. Longevity* **2016**, *2016*, 3897250.

(26) Pelicano, H.; Carney, D.; Huang, P. ROS stress in cancer cells and therapeutic implications. *Drug Resist. Updates* **2004**, *7*, 97−110.

(27) Sabharwal, S. S.; Schumacker, P. T. Mitochondrial ROS in cancer: initiators, amplifiers or an Achilles' heel? *Nat. Rev. Cancer* **2014**, *14*, 709−721.

(28) Durand, N.; Storz, P. Targeting reactive oxygen species in development and progression of pancreatic cancer. *Expert Rev. Anticancer Ther.* **2017**, *17*, 19−31.

(29) Pathania, D.; Kuang, Y.; Sechi, M.; Neamati, N. Mechanisms underlying the cytotoxicity of a novel quinazolinedione-based redox modulator, QD232, in pancreatic cancer cells. *Br. J. Pharmacol.* **2015**, *172*, 50−63.

(30) Pathania, D.; Sechi, M.; Palomba, M.; Sanna, V.; Berrettini, F.; Sias, A.; Taheri, L.; Neamati, N. Design and discovery of novel quinazolinedione-based redox modulators as therapies for pancreatic cancer. *Biochim. Biophys. Acta, Gen. Subj.* **2014**, *1840*, 332−343.

(31) Madak, J. T.; Neamati, N. Membrane permeable lipophilic cations as mitochondrial directing groups. *Curr. Top. Med. Chem.* **2015**, *15*, 745−766.

(32) Millard, M.; Gallagher, J. D.; Olenyuk, B. Z.; Neamati, N. A selective mitochondrial-targeted chlorambucil with remarkable cytotoxicity in breast and pancreatic cancers. *J. Med. Chem.* **2013**, *56*, 9170−9179.

(33) Madak, J. T.; Cuthbertson, C. R.; Chen, W.; Showalter, H. D.; Neamati, N. Design, synthesis, and characterization of brequinar conjugates as probes to study DHODH inhibition. *Chem. - Eur. J.* **2017**, *23*, 13875−13878.

(34) Ali, S.; Almhanna, K.; Chen, W.; Philip, P. A.; Sarkar, F. H. Differentially expressed miRNAs in the plasma may provide a molecular signature for aggressive pancreatic cancer. *Am. J. Transl Res.* **2010**, *3*, 28−47.

(35) Ouyang, H.; Mou, L.; Luk, C.; Liu, N.; Karaskova, J.; Squire, J.; Tsao, M. S. Immortal human pancreatic duct epithelial cell lines with near normal genotype and phenotype. *Am. J. Pathol.* **2000**, *157*, 1623−1631.

(36) Paulsen, M. T.; Veloso, A.; Prasad, J.; Bedi, K.; Ljungman, E. A.; Magnuson, B.; Wilson, T. E.; Ljungman, M. Use of Bru-Seq and BruChase-Seq for genome-wide assessment of the synthesis and stability of RNA. *Methods* **2014**, *67*, 45−54.

(37) Paulsen, M. T.; Veloso, A.; Prasad, J.; Bedi, K.; Ljungman, E. A.; Tsan, Y. C.; Chang, C. W.; Tarrier, B.; Washburn, J. G.; Lyons, R.; Robinson, D. R.; Kumar-Sinha, C.; Wilson, T. E.; Ljungman, M. Coordinated regulation of synthesis and stability of RNA during the

DOI: 10.1021/acs.jmedchem.7b01463
J. Med. Chem. 2018, 61, 1576−1594

acute TNF-induced proinflammatory response. *Proc. Natl. Acad. Sci. U. S. A.* **2013**, *110*, 2240−2245.
(38) Jaiswal, A. K. Nrf2 signaling in coordinated activation of antioxidant gene expression. *Free Radical Biol. Med.* **2004**, *36*, 1199−1207.
(39) Dinkova-Kostova, A. T.; Holtzclaw, W. D.; Cole, R. N.; Itoh, K.; Wakabayashi, N.; Katoh, Y.; Yamamoto, M.; Talalay, P. Direct evidence that sulfhydryl groups of Keap1 are the sensors regulating induction of phase 2 enzymes that protect against carcinogens and oxidants. *Proc. Natl. Acad. Sci. U. S. A.* **2002**, *99*, 11908−11913.
(40) Zhang, D. D.; Hannink, M. Distinct cysteine residues in Keap1 are required for Keap1-dependent ubiquitination of Nrf2 and for stabilization of Nrf2 by chemopreventive agents and oxidative stress. *Mol. Cell. Biol.* **2003**, *23*, 8137−8151.
(41) Alam, J.; Stewart, D.; Touchard, C.; Boinapally, S.; Choi, A. M.; Cook, J. L. Nrf2, a Cap'n'Collar transcription factor, regulates induction of the heme oxygenase-1 gene. *J. Biol. Chem.* **1999**, *274*, 26071−26078.
(42) Nioi, P.; McMahon, M.; Itoh, K.; Yamamoto, M.; Hayes, J. D. Identification of a novel Nrf2-regulated antioxidant response element (ARE) in the mouse NAD(P)H:quinone oxidoreductase 1 gene: reassessment of the ARE consensus sequence. *Biochem. J.* **2003**, *374*, 337−348.
(43) Ross, D.; Kepa, J. K.; Winski, S. L.; Beall, H. D.; Anwar, A.; Siegel, D. NAD(P)H:quinone oxidoreductase 1 (NQO1): chemoprotection, bioactivation, gene regulation and genetic polymorphisms. *Chem.-Biol. Interact.* **2000**, *129*, 77−97.
(44) Dinkova-Kostova, A. T.; Talalay, P. Persuasive evidence that quinone reductase type 1 (DT diaphorase) protects cells against the toxicity of electrophiles and reactive forms of oxygen. *Free Radical Biol. Med.* **2000**, *29*, 231−240.
(45) Choi, A. M.; Alam, J. Heme oxygenase-1: function, regulation, and implication of a novel stress-inducible protein in oxidant-induced lung injury. *Am. J. Respir. Cell Mol. Biol.* **1996**, *15*, 9−19.
(46) Shamu, C. E.; Walter, P. Oligomerization and phosphorylation of the Ire1p kinase during intracellular signaling from the endoplasmic reticulum to the nucleus. *EMBO J.* **1996**, *15*, 3028−3039.
(47) Harding, H. P.; Zhang, Y.; Bertolotti, A.; Zeng, H.; Ron, D. Perk is essential for translational regulation and cell survival during the unfolded protein response. *Mol. Cell* **2000**, *5*, 897−904.
(48) Haze, K.; Yoshida, H.; Yanagi, H.; Yura, T.; Mori, K. Mammalian transcription factor ATF6 is synthesized as a transmembrane protein and activated by proteolysis in response to endoplasmic reticulum stress. *Mol. Biol. Cell* **1999**, *10*, 3787−3799.
(49) Hetz, C. The unfolded protein response: controlling cell fate decisions under ER stress and beyond. *Nat. Rev. Mol. Cell Biol.* **2012**, *13*, 89−102.
(50) Kim, R.; Emi, M.; Tanabe, K.; Murakami, S. Role of the unfolded protein response in cell death. *Apoptosis* **2006**, *11*, 5−13.
(51) Verfaillie, T.; Garg, A. D.; Agostinis, P. Targeting ER stress induced apoptosis and inflammation in cancer. *Cancer Lett.* **2013**, *332*, 249−264.
(52) Nishitoh, H. CHOP is a multifunctional transcription factor in the ER stress response. *J. Biochem.* **2012**, *151*, 217−219.
(53) Oyadomari, S.; Mori, M. Roles of CHOP/GADD153 in endoplasmic reticulum stress. *Cell Death Differ.* **2004**, *11*, 381−389.
(54) Ghosh, A. P.; Klocke, B. J.; Ballestas, M. E.; Roth, K. A. CHOP potentially co-operates with FOXO3a in neuronal cells to regulate PUMA and BIM expression in response to ER stress. *PLoS One* **2012**, *7*, e39586.
(55) Jutooru, I.; Chadalapaka, G.; Lei, P.; Safe, S. Inhibition of NFkappaB and pancreatic cancer cell and tumor growth by curcumin is dependent on specificity protein down-regulation. *J. Biol. Chem.* **2010**, *285*, 25332−25344.
(56) Kasiappan, R.; Jutooru, I.; Karki, K.; Hedrick, E.; Safe, S. Benzyl isothiocyanate (BITC) induces reactive oxygen species-dependent repression of STAT3 protein by down-regulation of specificity proteins in pancreatic cancer. *J. Biol. Chem.* **2016**, *291*, 27122−27133.
(57) Jutooru, I.; Guthrie, A. S.; Chadalapaka, G.; Pathi, S.; Kim, K.; Burghardt, R.; Jin, U. H.; Safe, S. Mechanism of action of phenethylisothiocyanate and other reactive oxygen species-inducing anticancer agents. *Mol. Cell. Biol.* **2014**, *34*, 2382−2395.
(58) Guleng, G.; Lovig, T.; Meling, G. I.; Andersen, S. N.; Rognum, T. O. Mitochondrial microsatellite instability in colorectal carcinomas–frequency and association with nuclear microsatellite instability. *Cancer Lett.* **2005**, *219*, 97−103.
(59) Kabekkodu, S. P.; Bhat, S.; Mascarenhas, R.; Mallya, S.; Bhat, M.; Pandey, D.; Kushtagi, P.; Thangaraj, K.; Gopinath, P. M.; Satyamoorthy, K. Mitochondrial DNA variation analysis in cervical cancer. *Mitochondrion* **2014**, *16*, 73−82.
(60) Suzuki, M.; Toyooka, S.; Miyajima, K.; Iizasa, T.; Fujisawa, T.; Bekele, N. B.; Gazdar, A. F. Alterations in the mitochondrial displacement loop in lung cancers. *Clin. Cancer Res.* **2003**, *9*, 5636−5641.
(61) Wheelhouse, N. M.; Lai, P. B.; Wigmore, S. J.; Ross, J. A.; Harrison, D. J. Mitochondrial D-loop mutations and deletion profiles of cancerous and noncancerous liver tissue in hepatitis B virus-infected liver. *Br. J. Cancer* **2005**, *92*, 1268−1272.
(62) Lievre, A.; Chapusot, C.; Bouvier, A. M.; Zinzindohoue, F.; Piard, F.; Roignot, P.; Arnould, L.; Beaune, P.; Faivre, J.; Laurent-Puig, P. Clinical value of mitochondrial mutations in colorectal cancer. *J. Clin. Oncol.* **2005**, *23*, 3517−3525.
(63) Ye, K.; Lu, J.; Ma, F.; Keinan, A.; Gu, Z. Extensive pathogenicity of mitochondrial heteroplasmy in healthy human individuals. *Proc. Natl. Acad. Sci. U. S. A.* **2014**, *111*, 10654−10659.
(64) Na, H. K.; Surh, Y. J. Oncogenic potential of Nrf2 and its principal target protein heme oxygenase-1. *Free Radical Biol. Med.* **2014**, *67*, 353−365.
(65) Moon, E. J.; Giaccia, A. Dual roles of NRF2 in tumor prevention and progression: Possible implications in cancer treatment. *Free Radical Biol. Med.* **2014**, *79*, 292−299.
(66) Hayes, J. D.; McMahon, M. NRF2 and KEAP1 mutations: permanent activation of an adaptive response in cancer. *Trends Biochem. Sci.* **2009**, *34*, 176−188.
(67) Lister, A.; Nedjadi, T.; Kitteringham, N. R.; Campbell, F.; Costello, E.; Lloyd, B.; Copple, I. M.; Williams, S.; Owen, A.; Neoptolemos, J. P.; Goldring, C. E.; Park, B. K. Nrf2 is overexpressed in pancreatic cancer: implications for cell proliferation and therapy. *Mol. Cancer* **2011**, *10*, 37.
(68) Arlt, A.; Sebens, S.; Krebs, S.; Geismann, C.; Grossmann, M.; Kruse, M. L.; Schreiber, S.; Schafer, H. Inhibition of the Nrf2 transcription factor by the alkaloid trigonelline renders pancreatic cancer cells more susceptible to apoptosis through decreased proteasomal gene expression and proteasome activity. *Oncogene* **2013**, *32*, 4825−4835.
(69) Dhillon, H.; Chikara, S.; Reindl, K. M. Piperlongumine induces pancreatic cancer cell death by enhancing reactive oxygen species and DNA damage. *Toxicol Rep* **2014**, *1*, 309−318.
(70) Dorr, R. T.; Raymond, M. A.; Landowski, T. H.; Roman, N. O.; Fukushima, S. Induction of apoptosis and cell cycle arrest by imexon in human pancreatic cancer cell lines. *Int. J. Gastrointest. Cancer* **2005**, *36*, 015−028.
(71) Cohen, S. J.; Zalupski, M. M.; Modiano, M. R.; Conkling, P.; Patt, Y. Z.; Davis, P.; Dorr, R. T.; Boytim, M. L.; Hersh, E. M. A phase I study of imexon plus gemcitabine as first-line therapy for advanced pancreatic cancer. *Cancer Chemother. Pharmacol.* **2010**, *66*, 287−294.
(72) Malhotra, J. D.; Kaufman, R. J. Endoplasmic reticulum stress and oxidative stress: a vicious cycle or a double-edged sword? *Antioxid. Redox Signaling* **2007**, *9*, 2277−2293.
(73) Falkenberg, M.; Larsson, N. G.; Gustafsson, C. M. DNA replication and transcription in mammalian mitochondria. *Annu. Rev. Biochem.* **2007**, *76*, 679−699.
(74) Montoya, J.; Gaines, G. L.; Attardi, G. The pattern of transcription of the human mitochondrial rRNA genes reveals two overlapping transcription units. *Cell* **1983**, *34*, 151−9.
(75) Ojala, D.; Montoya, J.; Attardi, G. tRNA punctuation model of RNA processing in human mitochondria. *Nature* **1981**, *290*, 470−474.
(76) Subramanian, A.; Tamayo, P.; Mootha, V. K.; Mukherjee, S.; Ebert, B. L.; Gillette, M. A.; Paulovich, A.; Pomeroy, S. L.; Golub, T. R.;

DOI: 10.1021/acs.jmedchem.7b01463
J. Med. Chem. 2018, 61, 1576−1594

Lander, E. S.; Mesirov, J. P. Gene set enrichment analysis: a knowledge-based approach for interpreting genome-wide expression profiles. *Proc. Natl. Acad. Sci. U. S. A.* **2005**, *102*, 15545−15550.
(77) Mootha, V. K.; Lindgren, C. M.; Eriksson, K. F.; Subramanian, A.; Sihag, S.; Lehar, J.; Puigserver, P.; Carlsson, E.; Ridderstrale, M.; Laurila, E.; Houstis, N.; Daly, M. J.; Patterson, N.; Mesirov, J. P.; Golub, T. R.; Tamayo, P.; Spiegelman, B.; Lander, E. S.; Hirschhorn, J. N.; Altshuler, D.; Groop, L. C. PGC-1alpha-responsive genes involved in oxidative phosphorylation are coordinately downregulated in human diabetes. *Nat. Genet.* **2003**, *34*, 267−273.

DOI: 10.1021/acs.jmedchem.7b01463
J. Med. Chem. 2018, 61, 1576−1594